sustainability

MDPI

Article

A Phosphonic Functionalized Biopolymer for the Sorption of Lanthanum (III) and Application in the Recovery of Rare Earth Elements

Mohammed F. Hamza [1,2,*], Walid M. Abdellah [2], Doaa I. Zaki [2], Yuezhou Wei [1,3,*], Khalid Althumayri [4], Witold Brostow [5,6] and Nora A. Hamad [5,6,7]

1 School of Nuclear Science and Technology, University of South China, Hengyang 421001, China
2 Nuclear Materials Authority, El-Maadi, Cairo 11728, Egypt
3 School of Nuclear Science and Engineering, Shanghai Jiao Tong University, Shanghai 200240, China
4 Department of Chemistry, College of Science, Taibah University, Al-Madinah Al-Munawarah 30002, Saudi Arabia
5 Laboratory of Advanced Polymers & Optimized Materials (LAPOM), Department of Materials Science and Engineering, University of North Texas, 3940 North Elm Street, Denton, TX 76207, USA
6 Department of Physics, University of North Texas, 3940 North Elm Street, Denton, TX 76207, USA
7 Chemistry Department, Faculty of Science, Menofia University, Shebin El-Kom 32511, Egypt
* Correspondence: m_fouda21@usc.edu.cn (M.F.H.); yzwei@usc.edu.cn (Y.W.); Tel.: +20-111-668-1228 (M.F.H.); +86-771-322-4990 (Y.W.)

Abstract: Phosphonic acid functionalization of gellan gum and chitosan biopolymers was successfully performed. In the first step, the sorption was investigated using La(III) ions before testing for the recovery of rare earth elements (REEs) from pretreated industrial acidic leachate. The sorbent was characterized by Fourier-transform infrared (FTIR), scanning electron microscopy with energy dispersive X-ray analysis (SEM-EDX), thermogravimetric analysis (TGA), Brunauer–Emmett–Teller (BET), and pH of zero charge (pH_{PZC}) determination. FTIR and EDX results show efficient grafting of phosphoryl groups. The sorption was determined for the crude materials before functionalization (PGEG) and after phosphorylation (TBP-PGEG). More efficient sorption was seen for phosphorylated sorbent than for the crude composite. The sorption capacity is 0.226 mmol La g^{-1} for the PGEG while the value is 0.78 mmol La g^{-1} for the TBP-PGEG. We infer that phosphonate groups participate in the sorption. The most effective sorption is at pH = 4. The kinetic behavior was described using pseudo first-order equations (PFORE), pseudo second-order equations (PSORE), and resistance to intraparticle diffusion (RIDE). The sorption isotherms can be better represented by Langmuir and Sips equations than by the Freundlich equation. The sorbent shows high stability performance during reuse cycles with a limit on the decrease in the sorption performances and stability in the desorption performances. We have thus developed a good tool for the recovery of REEs with a selectivity higher than that of the non-functionalized components.

Keywords: biopolymer; phosphorylated sorbent; uptake kinetics; sorption isotherms; rare earth elements

Citation: Hamza, M.F.; Abdellah, W.M.; Zaki, D.I.; Wei, Y.; Althumayri, K.; Brostow, W.; Hamad, N.A. A Phosphonic Functionalized Biopolymer for the Sorption of Lanthanum (III) and Application in the Recovery of Rare Earth Elements. *Sustainability* **2023**, *15*, 2843. https://doi.org/10.3390/su15032843

Academic Editor: Munjed A. Maraqa

Received: 4 January 2023
Revised: 31 January 2023
Accepted: 1 February 2023
Published: 3 February 2023

1. Introduction

The recycling of materials and thus sustainability are increasingly important [1]. This applies also to the recovery of rare earth elements (REEs) [2]. Lanthanum is a light rare earth element with an atomic number of 57. It is found abundantly in the environment; it is a soft, malleable, ductile, and silver-white metal. Lanthanum is naturally found in sediments; it oxidizes rapidly in air and reacts with water to form the hydroxide. The salts of lanthanum are insoluble in water. It is used in the field of optics as lenses, the production of catalysts, the polishing of glass, and also in radiation absorbing glasses [3]. Like most other rare earth elements, the usual oxidation state is +3. It usually occurs together with

cerium and the other rare earth elements. It mainly occurs in monazite (Ce, La, Y, Th) PO_4 and bastnäsite (La, Ce)FCO_3 ores in measurable quantities [4].

Several procedures were used for the extraction of REEs from the secondary resources such as phosphate rocks [5], minerals with low-grade concentration [6], and wastes from industrial materials [7–9])). Hydrometallurgical techniques have been used for dissolving metal ions from solid materials to leachate solution [10–18]. Leachates are contaminated liquids generated from water percolating through a solid waste disposal site, accumulating contaminants, and moving into subsurface areas. Target metal ions have been obtained by solvent extraction or direct precipitation [19–25]. Both these methods were used for high-grade metal ions and are inefficient for low-concentration solutions. Some functional groups play a vital role in the extraction process, most of them based on phosphorus compounds such as alkylated phosphoric acid [26–28], phosphonate groups [3,20,29–32], extractants containing organo-phosphonic groups [33–36], ionic liquids with phosphonium [37,38], or alkylated phosphine oxide [39,40].

For the low-grade concentrations, precipitation and solvent treatment are not applicable; hence, the target metal ions are extracted through other processes. These techniques involve using an impregnated sorbent, for instance, in REEs for the enrichment and separation from acidic solutions. This technique is fast and has a high capacity [41–44]. Small-size nanoscale sorbents were used for the mitigation of mass transfer [45]. The incorporation of magnetite nano scale particles into polymer improves the kinetics and separation efficiency [46–48]. Other conventional adsorbents including chelating [41,49–51] and ion-exchange sorbents [52–56] have been used for recovering target metals from acidic and alkaline solutions. These materials have functional groups for binding with metal ions even present at low concentrations with high selectivity. Such sorbents include Purolite (C-100) [56] and Dowex (50W X8) [53]. Multi-functional sorbents with sulfonic, carboxylic, and diphosphonic groups [57] constitute the Purolite family [50].

High affinity of the phosphorus extractants towards REEs and fast process kinetics provided a basis for designing a number of solid phase adsorbents such as Tulsion (CH-96) and (T-PAR) resins [58,59], Tulsion (CH-93) [33], and Diphonix [60].

Chitosan particles are obtained from deacetylated chitin. Chitin appears naturally in the crustaceans such as crab, crayfish, shrimp shells, and cuttlefish, in insect cuticles, and cell walls of the fungi [61]. Chitin is well known because of its uses in water treatment (removal of pollution such as dyes or heavy metals). The abundance of hydroxyl and amine groups in its structures [62,63] makes this biopolymer a vital component in many adsorbents—with possibilities of further modification (chemically) by grafting of additional groups for increasing the capacity and selectivity, also by designing (physically) beads and nanomaterials for improving the kinetic properties. Moreover, the presence of such groups enables the reinforcement of the final products by crosslinking by binding with amines and hydroxyls [64–66].

Several studies were performed for metal recovery using modified chitosan particles. Crosslinked lanthanum-loaded chitosan/silica gel particles was performed through designing a $LaCl_3 \cdot 7H_2O$, chitosan and silica gel composite—which crosslinked using glutaraldehyde crosslinker yielding (LaSiCS), an excellent sorbent for chromium removal [67]. Another sorbent was synthesized and explored for the removal of lanthanum and lead ions from water using a manganese dioxide chitosan composite (crosslinked by formaldehyde). The sorbent shows a high affinity and rapid reaction with these ions [68]. Sorbents based on chitosan and polyvinylpyrrolidone (PVP) particles were designed for the separation of La(III) from (La(III), Ce(III), and Sm(III)). Tartaric acid with a concentration of 0.25 M was used as an eluent for lanthanide from Ln(III)IP-CS/PVP particles with a selective extraction capabilities [69].

In this work, the chitosan particles were coupled with gellan gum through crosslinking reagents (EPI and GA); functionalization was performed by phosphorylation through tributyl phosphate (TBP) and phosphoric acid (H_3PO_4). Both sorbents were characterized by FTIR, TGA, BET, pHpzc, and SEM-EDX analyses. The second part of this work involved

the determination of the sorption properties of sorbents toward La ions—including effects of pH, uptake kinetics, sorption isotherms (the sorption efficiency of the functionalized sorbent exceeding by more than three folds compared to the nonfunctionalized composite, with fast kinetic properties (25 min compared to 40 min)), and sorption from polymetallic equal molar solutions (with respect to the pH of the loaded solution). Finally, the last part of the study involved the recovery of REEs from an acidic leachate solution for the evaluation of sorbents toward natural solutions, which shows a high affinity toward the REE solution.

2. Materials and Methods

2.1. Materials

Gellan gum was supplied by Gino Biotech—Zhengzhou, Henan, China. Chitosan (medium molecular weight), glutaraldehyde ((GA)50%, *w*/*w* in water), and poly(vinyl alcohol) (PVA) with molecular wt. between 9000 and 10,000 (80% hydrolyzed) were supplied by Sigma-Aldrich (Shanghai) Trading Co. Ltd., Pudong, Shanghai, China. Tributyl phosphate ((TBP); $CH_3(CH_2)_3O)_3PO$, >99%, epichlorohydrin (EPI) C_3H_5ClO, 99% and phosphoric acid H_3PO_4, 99.99% were purchased from Shanghai-Makclin- Biochemical Co., Ltd. (Shanghai, China). Terbium (III) sulfate (used in the selectivity test) and lanthanum (III) sulfate were supplied by the Rare Earth (RE) Metallurgy and Functional Materials Co., Ltd., China (National Engineering Research Centre). Silicon (source of silica standard solution for selectivity experiments) with initial concentration of 1000 ppm was supplied by Guobiao-Inspection and Certification-Co. Ltd. Huairou-District, Beijing, China. The remaining reagents used in this study were Prolabo products, VWR, Radnor, PA, USA.

2.2. Synthesis Procedures

Phosphorylating agent was synthesized by addition of 25 g of TBP solution in a three-nicked round bottom flask—followed by addition of 8 mL phosphoric acid solution. The reactor was closed and the reaction mixture was refluxed at 80 °C for 1 h. After cooling, another addition to the mixture was 8 g of EPI; the solution was refluxed again for 4 h at 90 °C, then left for cooling (named as part A); see Scheme 1.

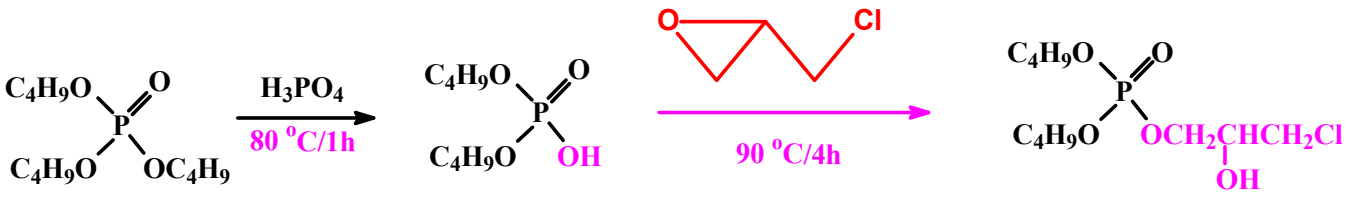

Scheme 1. Synthesis pathway of the phosphorylating agent.

A mixture of 1.2 g of gellan gum and 1.2 g of chitosan was dissolved in 30 mL of 5% acetic acid solution, then 10 mL of 2% PVA added under continued stirring until homogeneity was achieved. Then, EPI was added as crosslinker and the system left in an oven at 40 °C overnight. The material so produced is gelatinous (named as part B).

We have also made a non-functionalized material (1)—used in a comparable study of the sorption with the phosphorylated composite. The same procedure was repeated for B and continued by addition of EPI, then refluxed at 60 °C; the material was poured into a 500 mL solution of GA (15%) and stirred overnight before being filtered and dried to produce a precipitate (PGEG).

Scheme 2 shows the synthesis procedure of PGEG.

Addition of B to A was followed by refluxing for 12 h at 90 °C. The final product was obtained by pouring the mixture into a beaker containing 5% NaOH with 20 mL GA solution to provide a phosphorylated composite (Scheme 3). The mixture was stirred for 10 h at room temperature and the precipitated product was filtered and washed by water and acetone for removal of the unreacted substrates.

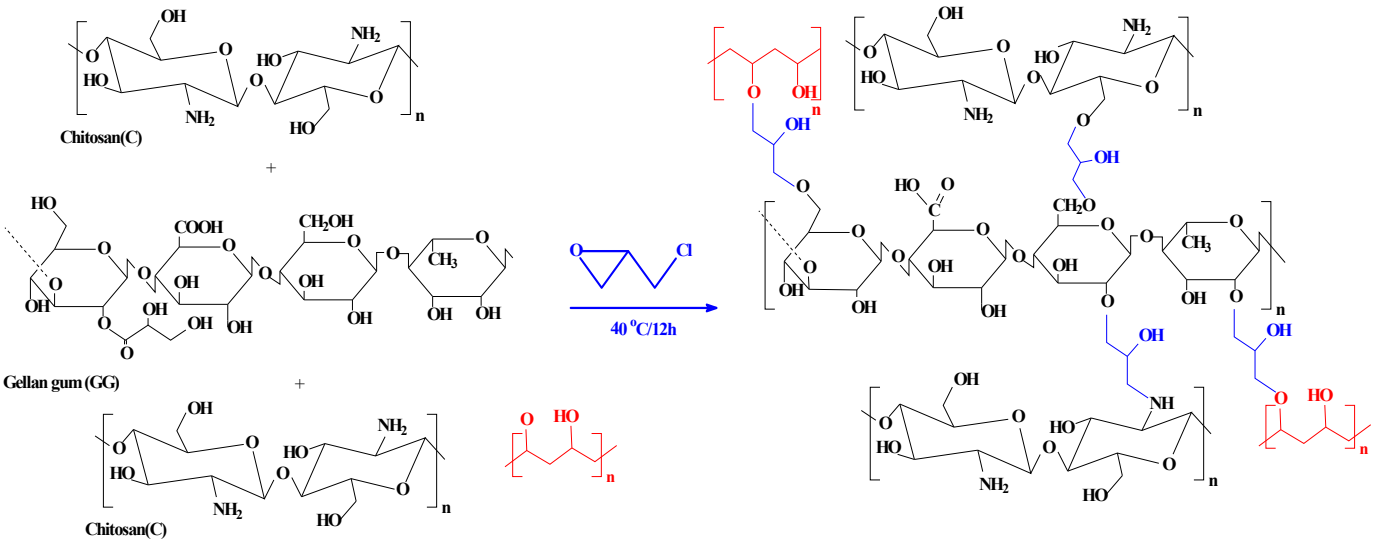

Scheme 2. Synthesis procedures of PGEG composite.

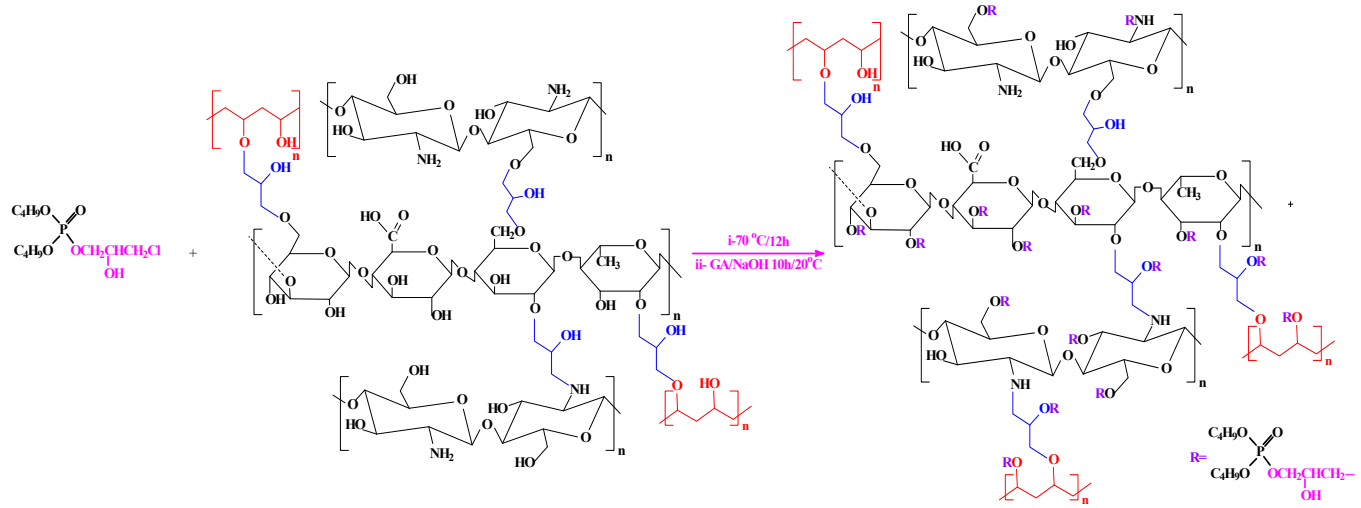

Scheme 3. Scheme of the phosphorylation method of PGEG (TBP-PGEG).

2.3. Characterization of Materials

FT-IR spectroscopy was performed using the IRTracer-100 (FT-IR spectrometer Shimadzu, Tokyo, Japan). Samples were dried at 65 °C for 10 h and ground with KBr (dried at 70 °C for 12 h) before creation of each disk for analysis. The pH_{PZC} values of both functionalized (TBP-PGEG) and non-functionalized (PGEG) products were determined with 0.1 M NaCl solution using the drift method [70]; the pH in this study ranged from 1 to 11 after keeping the samples for 48 h. The pore size and pore volume were determined using the nitrogen sorption desorption isotherms (Brunauer-Emmett-Teller or BET analysis). Both samples were treated with nitrogen gas for 5 h at 130 °C. SEM and EDX analyses were performed using Phenom, ProX-SEM, Thermo Fisher Scientific, Eindhoven, the Netherlands. Thermogravimetric analysis (TGA) was performed using Netzsch-STA, 449 F3-Jupiter, Netzsch Gerätebau-H Gmbh, Selb, Germany, performed in nitrogen atmosphere with the temperature increase rate of 10 °C min^{-1}. The pH of solutions was adjusted before sorption and measured after loading; this was also the case for the pH_{PZC} using a Compact (pH-S220-Seven/Ionometer) from Mettler-Toledo, Shanghai, China. The liquid samples including metal ions went through a filtrate membrane (1.2 µm) before testing for metals using the Inductively Coupled Plasma (ICP) analysis (ICPS; 7510-Shimadzu, Tokyo, Japan).

2.4. Metal Sorption Properties

The batch process was used in the sorption from either synthetic or natural leachate solutions. An amount of dry sorbent (m, g) was added to a volume of solution (V, L) that had a specific concentration of metal ions with initial concentration (C_0, mmol L^{-1}) at a certain pH value (resulting from the pH study). The shaking speed during the sorption process is approximately 170 rpm at the temperature T = 22 ± 2 °C. At the end of sorption, the samples were collected, filtered, and the metal content determined using the ICP equipment (C_{eq}, mmol L^{-1}). The capacity of the matrix (q_{eq}, mmol g^{-1}) was calculated using the following equation:

$$q_{eq} = (C_0 - C_{eq}) \times V/m \quad (1)$$

The sorbent concentration was determined in a solution with an equimolar concentration before application of a leaching solution containing REEs. The samples from kinetic experiments were used for kinetic elution through treatment with 0.5 M HNO_3. The sorption recycling was performed up to 5 cycles (water rinsing was systematically perfumed between each cycle), in which the sorption capacity and efficiency were determined for investigate the loss %. Tables S1 and S2 summarize the kinetic and isotherm sorption parameters, respectively; the kinetics were performed using PFORE, PSORE, and RIDE (pseudo first-/second-order rate equations, and resistance to intraparticle diffusion, respectively), while the sorption isotherms were fitted using Freundlich, Langmuir, and Sips equations. The fitting quality were determined using R^2 (determination coefficient, also called squared multiple correlation coefficient) and AIC (the Akaike Information Criterion) [71]. The applied natural liquor was collected after pretreated acidic leaching of ore material after treatment for U recovery. The original leaching liquor with 410 mg REE L^{-1} and 530 mg U L^{-1} as appeared in Table S3 was firstly treated with amberlite IRA 400; the uranium decreased to 38 mg U L^{-1} with efficiency (sorption) around 93%. However, the REE(III) decreased to 380 mg L^{-1} with efficiency up to 7.3%. The other elements were reported in Table 1

Table 1. Constituents of solutions after treatment for uranium (VI) removal.

Constituent	Conc. (mg/L)	Constituent	Conc. (mg/L)
U	38	Al_2O_3	1896
REE	380	Pb	16.2
Fe	1852	Zr	15

3. Results

3.1. Sorbent Characterization

3.1.1. Textural Properties (BET Analysis and Morphological (SEM) Observations)

The composite after functionalization (TBP-PGEG) shows an increase of the specific surface area (SSA) equal to 22.15 m^2 g^{-1} when compared to 17 m^2 g^{-1} for the PGEG. The porous volume is higher as well, namely, 0.014 cm^3 g^{-1} for PGEG, while it is 0.068 cm^3 g^{-1} for TBP-PGEG. This comparison results from the isotherms of adsorption–desorption. The cumulative pores volume was increased by functionalization from 0.049 to 0.058 cm^3 g^{-1}.

3.1.2. SEM-EDX and Elemental Analysis

The SEM analysis shows an irregular shape with small pores of sorbents. Figure 1a,b shows the SEM morphological structure of both sorbents—smaller pores in functionalized sorbent than in the pristine composite. Figure 1c,d shows the EDX analysis of both sorbents; an increase of O contents from 45.5 to 46.31% and the appearance of 3.11% P in the functionalized sorbent confirm the successful modification on the PGEG composite.

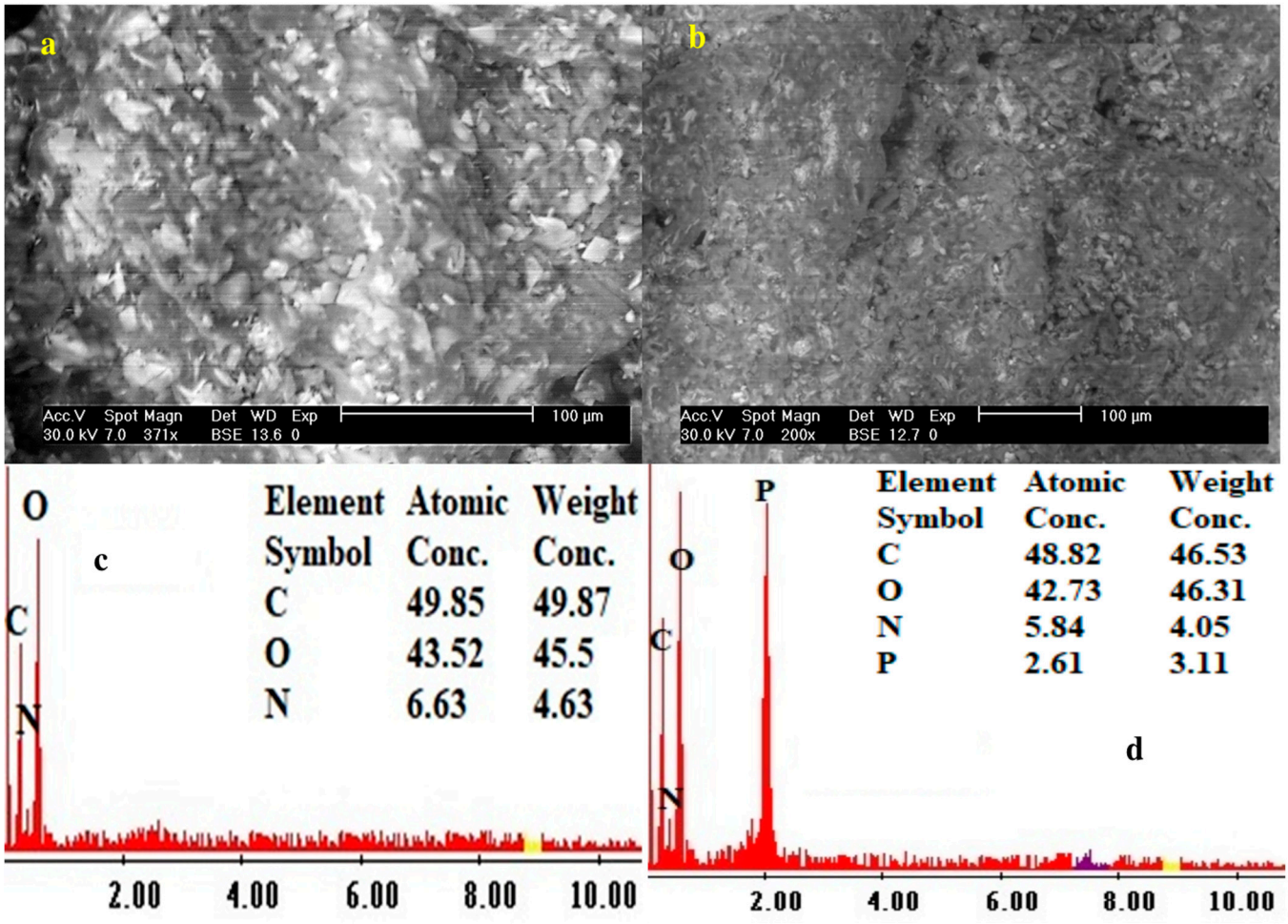

Figure 1. The surface morphological structure (SEM) and chemical composition (EDX) of PGEG (**a**,**c**) and TBP-PGEG (**b**,**d**) sorbents.

These results are confirmed by the elemental analysis of both PGEG and TBP-PGEG; see Table 2. As already noted, efficient phosphorylation is seen in an increase of the O% concentration and in the appearance of P in the functionalized sorbent. The O% concentration increases only a little, from 40.68 to 41.72% for the PGEG and TBP-PGEG, respectively, while the P appears with 4.83%.

Table 2. The elemental analysis results for PGEG and TBP-PGEG composites.

Sorbent	C [%]	N [%]	H [%]	O [%]	P [%]
PGEG (%)	47.56	4.78	6.98	40.68	0
PGEG (mmol)	39.60	3.41	69.26	25.43	0
TBP-PGEG (%)	42.14	4.13	7.18	41.72	4.83
TBP-PGEG (mmol)	35.09	2.95	71.24	26.08	1.56

3.1.3. Thermal Decomposition Analysis

Both sorbents show very similar thermal decomposition profiles in the TGA, with the percentage weight loss and the thermal stability shown in Figure 2. The weight loss of the sorbent values is 97.77 and 88.15% for PGEG and TBP-PGEG, respectively. The hydrocarbon concentration increases accordingly. Three loss profiles are seen for the sorbents—as discussed below.

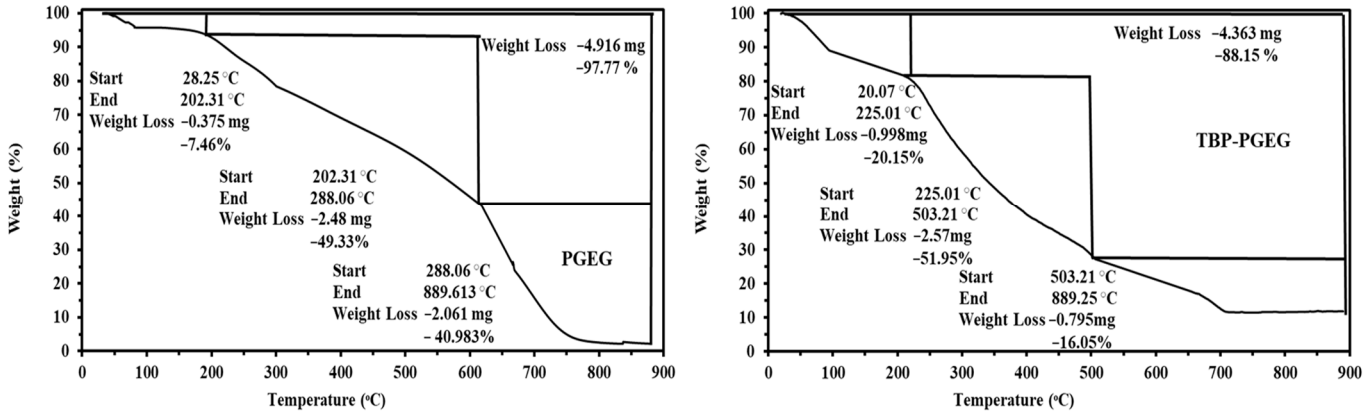

Figure 2. Thermogravimetric (TGA) analysis of the PGEG and TBP-PGEG sorbents.

The first stage is seen at 202 and 225 °C for PGEG and TBP-PGEG, respectively; this stage is due to the water loss (7.46 and 20.15 %, respectively) [72,73].

The second loss stage is seen below 288 and 503 °C for both sorbents, respectively. This stage is due to degradation of amines, cleavage of the crosslinking linkages, and decomposition of the network frames [74]. At this stage, there is a further weight loss, by 49 and 51% for both sorbents, respectively, followed by the final loss around 41 and 16%, respectively—due to depolymerization of the remaining hydrocarbon and to the char formation.

The Differential Thermogravimetric Analysis (DrTG) (Figure S1) for PGEG shows a series of peaks around 66, 139, 219, and 761 °C and two peaks for TBP-PGEG around 411 and 785 °C. We conclude that the phosphorylation reaction results in the successful grafting of the phosphonic groups and in achieving higher thermal stability.

3.1.4. FTIR Spectroscopy

Figure 3a,b shows a comparison of both sorbents before and after functionalization. We see the results for the sorbent after loading with La(III) and after five cycles of sorption and desorption.

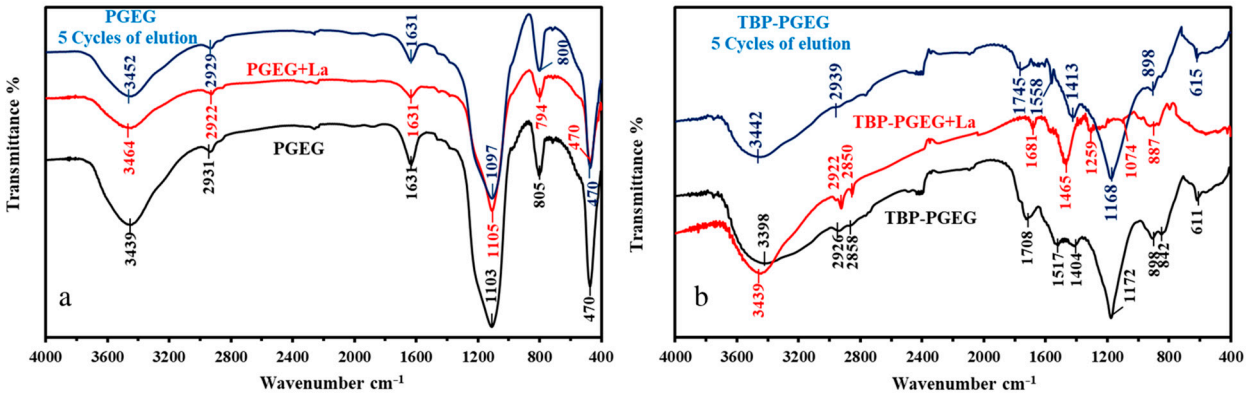

Figure 3. FTIR analysis of PGEG (**a**) and TPB-PGEG (**b**), after loading with La and after 5 cycles of sorption desorption.

The FTIR results confirm the structure of PGEG and TBP-PGEG sorbents. Both sorbents show peaks of OH and NH. Extra peaks are seen after phosphorylation reactions due to a change of the environment of these groups as reported in Table S4.

Briefly, we see a displacement of these peaks and changes in the peaks shape [75,76]. In addition, some new peaks are seen for the grafted moieties [77–82]; a peak at 1708 cm^{-1} and 1404 cm^{-1} for C=O and P=O, respectively [83] with a displacement of the NH peak

from 1630 cm^{-1} to 1517 cm^{-1}; a new peak at 1172 cm^{-1} for the P–O–C; a change in the shape of the peak at 805 cm^{-1} now divided into two parts at 842 cm^{-1} and 898 cm^{-1} for P–C groups [81,83]; and a change in the width of the peak at 611 cm^{-1} for the TBP-PGEG (the overlapping of P–O and Fe–O peaks) [84]. After metal sorption, some peaks, especially for OH, NH, and C=O, disappeared or shifted—apparently, because of the metal sorption [84–87]. The peaks in the 2800–1950 cm^{-1} range [88,89] correspond to the asymmetric aliphatic C–H. The peak at 1631 cm^{-1} in the pristine sorbent becomes split into two parts around 1700–1750 cm^{-1}—an effect of phosphorylation on the C=O environment while another peak appears at 1510–1580 cm^{-1} for the NH amine groups [90]. Phosphorylation is followed by peak broadening in the region of 800–1600 cm^{-1}—mainly due to the NH, C=O, P–O–C, P=O, P–C, and COO^- [90]. The changes after grafting and the shifts resulting from metal loading are discussed in Table S4, while Figure S2 shows a comparison of the spectra.

3.1.5. pH_{PZC} Analysis

Another evidence of the modifications on the PGEG surface including the presence of the solvent is the change of the pH with respect to pH_0. Figure S3 shows a comparison of the pH_{PZC} for PGEG and after functionalization. We see that the pH shifts toward higher values. The original components in the PGEG are amines (from chitosan) with pKa = 4.5 for the primary amine, 6.7 for the secondary amine, and 11.6 for the tertiary amine. Clearly, the acid base characteristics is affected by the phosphorylation progress. Kołodyńska and her colleagues [91] studied the progress of sorption in a series of resins with lanthanum; they reported pH_{PZC} values in the range from 8.13 to 9.93 for the aminophosphonic resins.

3.2. Detection in Synthetic Solutions

3.2.1. Effect of pH

Figure 4a–c shows a comparable study of La(III) sorption using PGEG and TBP-PGEG sorbents. Figure 4a shows the effect of pH on sorption at a pH_0 ranging from 1 to 6. The sorbents provide similar profiles, with a low sorption capacity at lower pH values then increasing gradually until saturation. For TBP-PGEG at lower pH values, the functional groups are protonated; these positively charged groups repulse the positively charged metal ions. The average loading capacity after saturation is 0.226 mmol La g^{-1} and 0.78 mmol La g^{-1} for PGEG and TBP-PGEG, respectively. This reflects the successful grafting of phosphonate groups; the loading capacity is higher than that of the pristine sorbent by ≈3.5 times. TBP-PGEG has high capacity in the entire pH range; both sorbents show the saturation equilibrium at pH = 4.

Figure 4b shows the variation of the pH through La(III) sorption. The pH changes by 0.3 units from the initial concentration and a little higher especially for the high pH values. We show in Figure 4c the plot of $\log_{10}$ of the D (distribution ratio = q_{eq}/C_{eq}) vs. pH_{eq}. We recall that q_{eq} has been defined in Equation (1). We see in Figure 4c that the plot is approximately linear, with the slope ≈ +0.49. Apparently, the metal ions are bound to the sorbent through chelation. The sorbent is partially deprotonated and the binding occurs through the lone pairs of electrons localized on atoms.

Figure S4 shows relative concentrations of La containing components as functions of pH. $LaSO_4^+$ has the highest concentration below pH = 4, coexisting in that pH range with the free cationic species La^{3+}. The anionic species in disulfate form $La(SO_4)_2^-$ is seen at pH < 3. The sorbents are partially protonated; the pH_{PZC} is ≈6.17 and ≈6.64 for PGEG and TBP-PGEG, respectively; this is evidence for binding free electrons to the positively charged metal ions—what explains the decreasing repulsion between functional groups and metal ions. The binding is achieved through OH, NH, COOH, and phosphonic groups—providing high loading capacity. This is verified by a decrease and displacement of these peaks after sorption; see again the FTIR spectra.

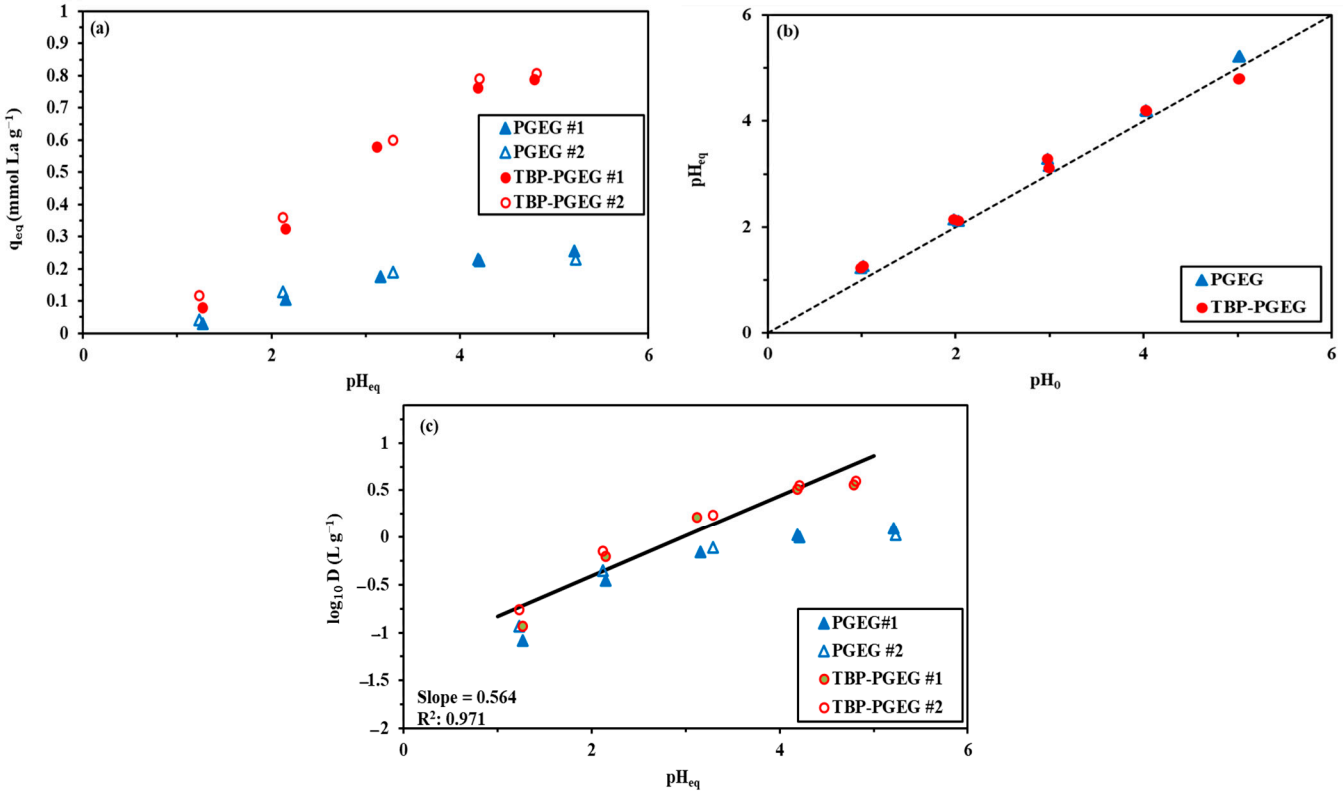

Figure 4. Effects of pH on sorption capacity of La (**a**), pH variation (**b**) and plot of $\log_{10}D$ against pH_{eq} (**c**).

Figure 5 shows the EDX diagrams of the loaded sorbents. The S element reflects the sorption of the sulfate species; the presence of P after grafting verifies the successful phosphorylation reaction while the high contents of La in TBP-PGEG shows a high loading capacity of the phosphonate sorbent compared to the crude one.

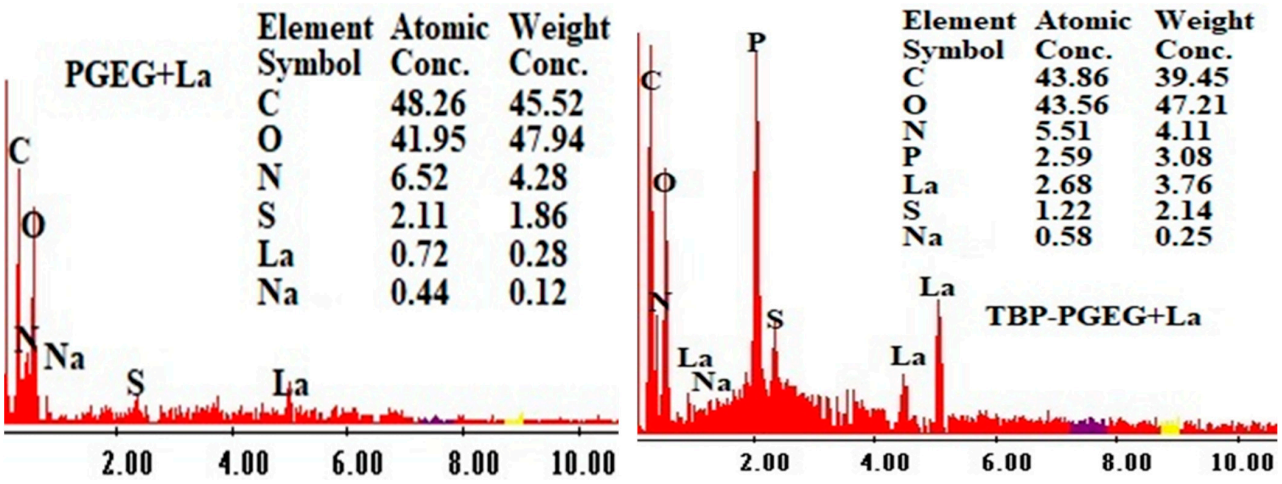

Figure 5. EDX analysis of PGEG and TBP-PGEG after La sorption.

3.2.2. Uptake Kinetics

The uptake kinetics depends on a variety of factors, including resistance to diffusion—which is different in film than in bulk, and there is also intraparticle diffusion. The homogeneity distribution of the sorbent particles depends on the agitation velocity and also on the film and bulk diffusion. The uptake kinetics was investigated considering PFORE,

PSORE, and RIDE (using the Crank equation). PFORE (usually reflecting the physical adsorption) provides a very good fit seen in Figure 6, while Figure S5—left shows the experimental and PSORE results related to chemical adsorption and Figure S5—right shows the experimental and RIDE results. Goodness of the fit of the R^2 and AIC values are provided in Table 3. The equilibrium was achieved at 40 and 25 min for PGEG and TBP-PGEG, respectively. Another advantage of grafting phosphoryl groups is the accelerated kinetics of sorption. This is related to the high affinity of phosphonate groups to REEs [92].

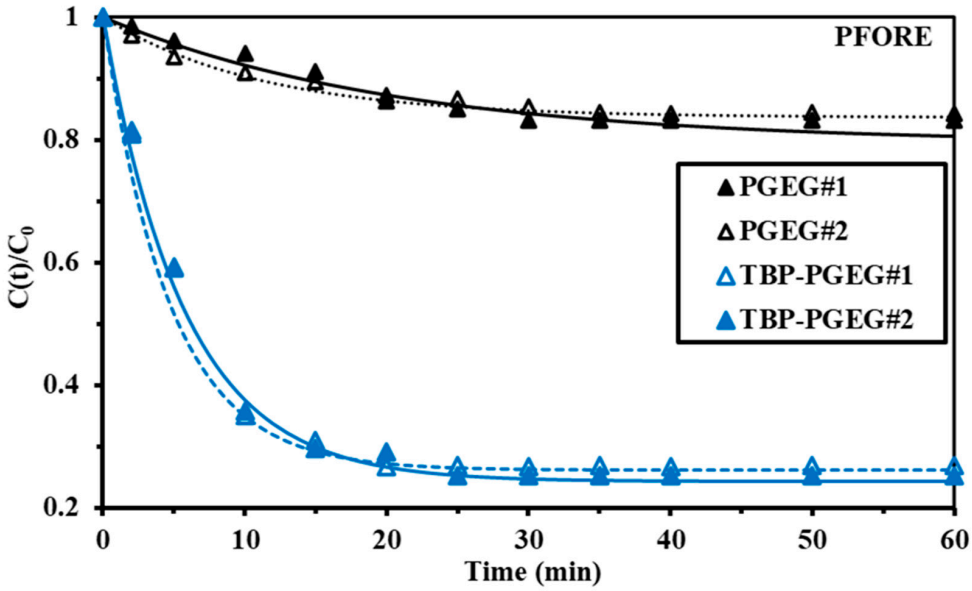

Figure 6. Kinetic profile of the fitted equation (PFORE) of the experimental data for La sorption of PGEG and TBP-PGEG sorbents at pH_0 = 5.

Table 3. Modeling of La(III) uptake kinetics for PGEG and TBP-PGEG sorbents at pH_0 = 5.

Model	Sorbent	PGEG		TBP-PGEG	
	Parameter	**1**	**2**	**1**	**2**
	$q_{eq,exp.}$	0.191	0.184	0.793	0.785
PFORE	$q_{eq,1}$	0.186	0.177	0.789	0.775
	$k_1 \times 10^2$	3.273	3.443	4.54	4.73
	R^2	0.995	0.985	0.983	0.989
	AIC	−125.1	−132.1	−133.7	−145.3
PSORE	$q_{eq,2}$	0.218	0.223	0.947	0.856
	$k_2 \times 10^2$	2.01	1.97	2.847	2.11
	R^2	0.921	0.913	0.935	0.927
	AIC	−21	−31	−39	−38
RIDE	$D_e \times 10^{13}$	1.36	1.49	2.06	2.25
	R^2	0.932	0.941	0.921	0.923
	AIC	−41	−44	−54	−57

Units: q_{eq}: mmol g^{-1}; k_1: min^{-1}; k_2: L $mmol^{-1}$ min^{-1}; D_e: m^2 min^{-1}.

3.2.3. Sorption Isotherms

The sorption isotherms show among others the maximum sorption capacity and the affinity toward the target metal ions. Different equations were used for representing the isotherms: (a) Langmuir was used for monolayer system without chemical interactions of the sorbed molecules—that is, for homogeneous sorption, good results are seen in Figure 7; (b) Freundlich, known to be used for multi-layer-sorption, a power-type equation, provides a worse fit than the Langmuir equation; and (c) Sips, which is a combination of

Freundlich and Langmuir equations with an additional third parameter, provides a good fit—as also seen in Figure 7. It seems noteworthy that the slope of the TBP-PGEG curve steeply increases before saturation—while this is not the case for PGEG. The total sorption of PGEG is ≈ 0.45 mmol La g^{-1} while it is ≈ 1.47 mmol La g^{-1} for the TBP-PGEG (a strong increase after phosphorylation).

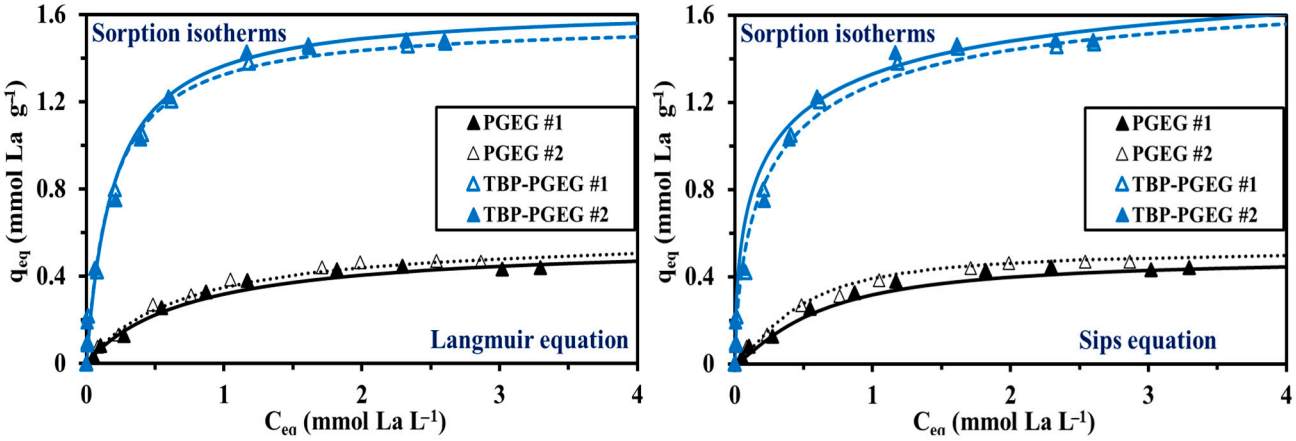

Figure 7. Experimental results and values calculated from Langmuir and Sips equations for the sorption isotherms of La(III) ions on PGEG and TBP-PGEG sorbents.

Figure S6 shows the bad-fitting profile (Freundlich) for both sorbents at pH_0 4. It is noteworthy that the slope of TBP-PGEG is steeply increased before saturation, while the PGEG profiles show a smooth increasing of the sorption under the same conditions. The total sorption of PGEG is around 0.45 mmol La g^{-1} comparing to 1.47 mmol La g^{-1} for the TBP-PGEG, which confirmed a strong increasing in the sorption capacities (increasing of three-fold after phosphorylation).

Table 4 reports the model's parameters with the statistical indicators of AIC and R^2. The high affinity of TBP-PGEG toward REEs can be related to the Pearson's rules, also called Hard&Soft Acid–Base Theory (HSAB) [93,94]. The phosphonate groups are classified as hard bases [95], which are attracted to the hard acids such as REEs. Series of phosphonate grafted sorbents were investigated toward different metal ions in which the hydrogen bond should be yield to establish the optimization of the binding properties [96].

Table 4. Modeling of La(III) sorption isotherms for PGEG and TBP-PGEG sorbents at pH_0 = 4.

Model	Sorbent		PGEG		TBP-PGEG	
	Parameter	Run	1	2	1	2
Experimental	$q_{m,exp.}$		0.433	0.471	1.457	1.483
Langmuir	$q_{m,L}$		0.439	0.477	1.475	1.489
	b_L		4.1	4.4	5.75	5.43
	R^2		0.982	0.987	0.994	0.991
	AIC		−54	−57	−77	−78
Freundlich	k_F		0.457	0.473	1.53	1.62
	n_F		2.18	2.59	3.88	4.17
	R^2		0.911	0.884	0.946	0.915
	AIC		−21	−18	−24	−28
Sips	$q_{m,S}$		0.435	0.463	1.461	1.487
	b_S		6.85	5.94	2.18	1.97
	n_S		1.04	1.12	1.17	1.13
	R^2		0.982	0.989	0.993	0.997
	AIC		−60	−53	−67	−69

Units: q_m: mmol g^{-1}; b_i: L $mmol^{-1}$; $n_{F/S}$: dimensionless; k_F: $L^{1/nF}$ $mmol^{1-1/nF}$ g^{-1}.

Table 5 reports the sorption performances of alternative sorbents for the extraction of La(III) and comparison with the results from using PGEG or TBP-PGEG sorbents. The difference in the conditions makes such a comparison only an approximation. However, we see meaningful trends through comparison of the sorption capacities, b_L, and equilibrium times. The TBP-PGEG is characterized by fast kinetics and highly sorption properties compared to the PGEG and most sorbents known from the literature. Functionalized-chitosan [97], alginate magnetite beads [98], MOF functionalized sorbent [99], and POH-A_LPEI [100] show high sorption capacities while TBP-PGEG positively distinguishes itself by its fast kinetics.

Table 5. La(III) sorption for alternative sorbents.

Sorbent	Time	pH_0	$q_{m,L}$	b_L	Ref.
Mycobacterium-smegmatis	180	1.5	0.024	4.1	[101]
Citrus reticulata peel	60	5	1.11	10.6	[102]
Lewatit TP-207	60	3.6	0.867	47.0	[103]
Functionalized membrane of calixarene	1440	5	1.12	144	[104]
Functionalized chitosan	240	4	2.03	0.06	[97]
SQS-6 cationic sorbent in H_3PO_4	10	4	0.086	3.66	[105]
Iron oxide-alginate	1680	5	0.861	0.563	[106]
Turbinaria-conoides	120	5	1.11	5.28	[107]
Sargassum-polycystum	n.d.	5	0.98	69.4	[108]
Grapefruit peel	60	5	1.23	5.21	[109]
Platanus orientalis leaf	60	4	0.206	18.1	[110]
SnO_2-TiO_2 nanocomposites	60	5	0.488	26.4	[111]
Sargassum (sp).	60	n.d.	0.66	116	[112]
Alginate magnetite beads	300	4	2.03	0.87	[98]
Bamboo-charcoal	480	7.2	1.38	76.5	[113]
Banana peel	1440	5.2	0.279	361	[114]
Magnetic graphene nanoparticles	15	4	0.358	35.4	[115]
Purolite-S950	180	0.2M HNO_3	0.636	12.9	[91]
MOF functionalized sorbent	40–60	7	2.08	44.4	[99]
Pseudomonas aeruginosa	180	5	1.00	n.d.	[116]
A_LPEI	40	5	0.573	1.14	[100]
POH-A_LPEI	40	5	1.61	3.85	[100]
PGEG	40	4	0.45	4.3	*This work*
TBP-PGEG	25	4	1.47	5.6	*This work*

Units: Time: min, $q_{m,L}$: mmol g^{-1}; b_L: L $mmol^{-1}$.

3.2.4. Multi-Component Solutions—Selectivity

Supplementary studies of the experiments were focused on the treatment of La with equimolar polymetallic ions. Prepared equimolar solutions of La, Si, Ca, Mg, and Tb (heavy rare earth elements) were used to investigate the selectivity behavior of the TBP-PGEG in polymetallic solution; most of these ions coexist with La in a leachate solution. These experiments were performed for a pH_0 between 1 and 5. Figure 8a reports the selectivity of La against selected elements at different pH values—confirming the preference of sorbent for REEs over the major elements, especially so at higher pH values. The selectivity is in the order Si >> Mg > Ca >> Tb at pH_{eq} = 4.03, with values 49.3, 31.3, 22.9, and 2.4%, respectively. This confirms the high selectivity of the sorbent toward the associated elements and poor selectivity for other REEs. Figure 8b shows the loading capacity of metal ions at different stages which shows individual capacities as follows: 0.085, 0.128, 0.17, 0.53, and 0.65 mmol M g^{-1}; here M = Si, Mg, Ca, Tb, and La, respectively.

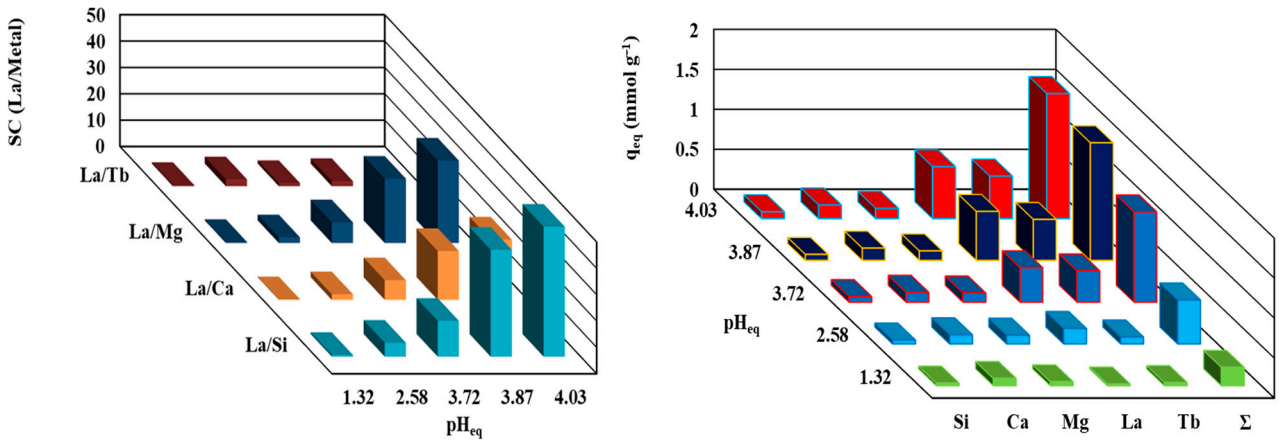

Figure 8. The selectivity (**a**) and the loading capacity (**b**) of TBP-PGEG in polymetallic solutions.

3.2.5. Desorption and the Sorbent Recycling

The desorption processes of adsorbed La(III) was studied in 20 mL of a 0.5 M HNO_3 solution with 100 mg of each sorbent. The desorption was faster than the adsorption. 20 and 15 min are sufficient for total desorption for PGEG and TBP-PGEG, respectively. These experiments were performed on samples collected from kinetic experiments. Five cycles of sorption were performed. A decrease in the loading capacity for the functionalized sorbent (not exceeding 3.5%) is seen after five cycles, while the desorption efficiency remains around 100%. Table 6 shows the performances of sorption and desorption for TBP-PGEG during the five cycles. S.D. is the standard deviation, R = removal, and De% = desorption in %.

Table 6. Sorption desorption performances for the TBP-PGEG sorbent.

	Sorption		Desorption	
Cycles	**Efficiency (%)**	**S.D. (Rem.%)**	**Efficiency (%)**	**S.D. (Des%)**
1	85.47	1.15	99.99	0.074
2	84.69	1.21	99.98	0.44
3	82.53	0.90	99.96	0.22
4	81.98	0.83	100.00	0.19
5	81.29	0.74	99.64	0.36

3.3. Applications

An acidic leaching solution was collected each time after being pretreated for U removal; the concentrations of metal ions in the solution were listed above in Table 1. The treatment was performed via both sorbents at different pH values. The concentration of REEs in the original solution was around 410 mg REE L^{-1} and decreased to 380 mg REE L^{-1} after a treatment with quaternary ammonium chloride resin for U(VI) removal with efficiency loss of 7.3%.

Figure 9a,b shows the selectivity performance of La(III) with respect to the metal ions of interest. The figure shows a variety in behaviors. As the pH increases, the sorption of metal ions increases with increasing selectivity as well. Better performance of the TBP-PGEG sorbent towards REEs is seen than that of the PGEG. The selectivity toward metal ions depends on the pH value. In case of PGEG, the maximum reached at pH_{eq} = 5.11 for Mg (SC/5.8), Ca (SC/4.46), Si(SC/2.5), and V (SC/2.3), while at pH_{eq} = 3.28, it reached maximum for Mn(SC/12.12), Fe(SC/7.35), and Al(SC/4.42). In the case of TBP-PGEG, it was noticed mainly at pH_{eq} = 4.79 for Ca (SC/93.7) > Mg (SC/89.9) > Mn(SC/60.1) >> Si(SC/23.7) > V (SC/17.0), while the SC of Al reached maximum at pH_{eq} = 4.09 with value 26.3 and Fe at pH_{eq} = 3.18 with value 48.5.

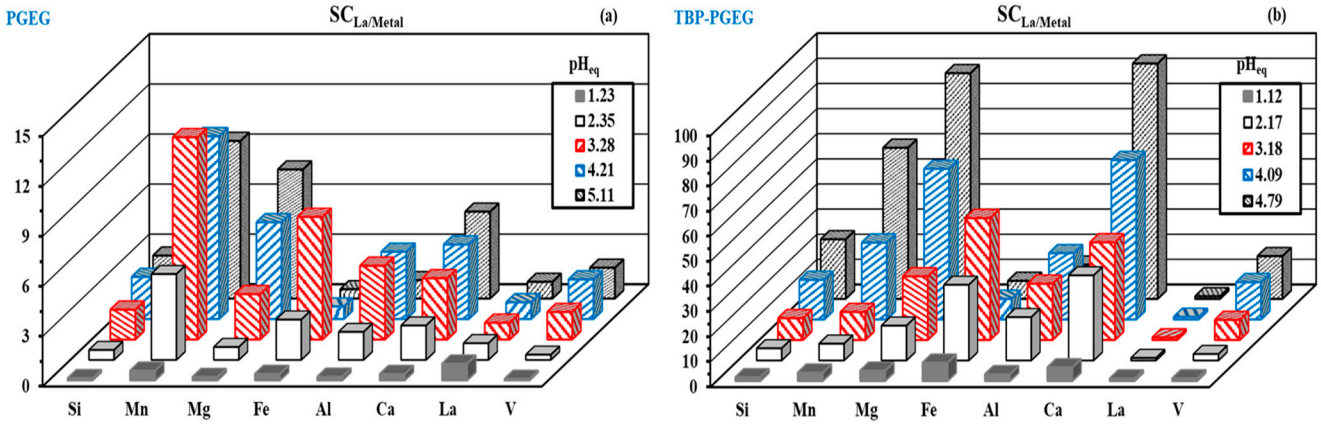

Figure 9. Selectivity performance of La vis metal ions for PGEG (**a**) and TBP-PGEG (**b**).

4. Conclusions

We have successfully synthesized new hydrogels based on gellan gum and chitosan for pristine polymer (PGEG) and for a functionalized polymer containing phosphonate groups (TBP-PGEG). The new sorbents have been fully characterized by FTIR, TGA, BET, SEM-EDX, and pH_{PZC}. The new functionalized sorbent was efficient for the recovering of REEs in a mild acidic solution and also for the recovering of REEs from a leachate solution. The partial deprotonation of functional groups at pH = 4 (amine, hydroxyl, phosphonate, and carboxylate) improves the sorption of REEs. Fast kinetics of the functionalized phosphonate sorbent is seen in the PFORE profile, 25 min rather than 40 min for PGEG. Elution was efficient using 0.5 M HNO_3 and the total desorption was achieved in 15 min for both sorbents. The Langmuir and Sips isotherms profiles provide better fits for both sorbents than the Freundlich equation. The maximum sorption capacities are 0.45 and 1.47 mmol La g^{-1} for PGEG and TBP-PGEG, respectively. It shows a high stability for sorption desorption with a slight drop after five cycles. The functionalized sorbent shows a high selectivity toward REEs in treatments of an equimolar synthetic solution (with selectivity 49.3, 31.3, 22.9, and 2.4% for Si, Mg, Ca, and Tb, respectively). The selectivity after the treatment of ore leachate was found to depend on the pH. For PGEG, the maximum selectivity was found at pH_{eq} = 5.11 for Ca and Mg, at pH_{eq} = 4.21 for Si and V, and at pH_{eq} = 3.28 for Mn, Fe, and Al. As for TBP-PGEG, the maximum selectivity occurred at pH_{eq} = 4.79 for Ca, Mg, Mn, Si, and V, while it was at pH_{eq} = 4.09 for Al and at pH_{eq} = 3.18 for Fe.

Supplementary Materials: The following supporting information can be downloaded at: https://www.mdpi.com/article/10.3390/su15032843/s1, Table S1: Equations used for modeling sorption isotherms [117–119]; Table S2: Equations used for modeling uptake kinetics [120,121]; Table S3: Constituents of leaching solution before used for U removal at (pH = 0.3); Table S4: FTIR assignments of peaks for PGEG, TBP-PGEG, after loading with La, and after 5 cycles of sorption desorption; Figure S1: Dr-TG analysis of the PGEG and TBP-PGEG sorbents; Figure S2: FTIR of collected spectra focusing on the main peaks [79–81,122–148]; Figure S3: pHpzc values of the PGEG and TBP-PGEG sorbents; Figure S4: Speciation of La at different pH values; Figure S5: PSORE (**a**) and RIDE (**b**) fitting curves of PGEG and TBP-PGEG sorbents; Figure S6: Freundlich equation fitting curves for the sorption isotherms of La(III) ions on PGEG and TBP-PGEG sorbents.

Author Contributions: Conceptualization, M.F.H., W.M.A. and D.I.Z.; methodology, M.F.H. and N.A.H.; software, D.I.Z. and Y.W.; validation, M.F.H., Y.W., K.A. and W.B.; formal analysis, M.F.H., D.I.Z., Y.W. and N.A.H.; investigation, K.A. and W.B.; resources, M.F.H., W.M.A., D.I.Z. and N.A.H.; data curation, K.A., W.B. and N.A.H.; writing—original draft preparation, W.B., M.F.H. and D.I.Z.; writing—review and editing, M.F.H.; visualization, K.A., W.B. and N.A.H.; project administration, Y.W.; funding acquisition, Y.W. All authors have read and agreed to the published version of the manuscript.

Funding: The National Natural Science Foundation of China for supporting projects [U1967218, and 11975082].

Institutional Review Board Statement: Not applicable.

Informed Consent Statement: Not applicable.

Data Availability Statement: Data/samples can be obtained from Authors on demand.

Acknowledgments: Y.W. acknowledges the National Natural Science Foundation of China for supporting the projects [U1967218, and 11975082].

Conflicts of Interest: The authors declare no conflict of interest.

References

1. Brostow, W.; Lobland, H.E.H. *Materials: Introduction and Applications*; John Wiley & Sons: Hoboken, NJ, USA, 2016.
2. Tasaki, K. A novel thermal hydrolysis process for extraction of keratin from hog hair for commercial applications. *Waste Manag.* **2020**, *104*, 33–41. [CrossRef] [PubMed]
3. Sinha, S.; Abhilash; Meshram, P.; Pandey, B.D. Metallurgical processes for the recovery and recycling of lanthanum from various resources—A review. *Hydrometallurgy* **2016**, *160*, 47–59. [CrossRef]
4. Ruan, C. Review of weathered crust rare earth ore. *J. Chin. Soc. Rare Earths* **2007**, *25*, 641.
5. Wu, S.; Wang, L.; Zhao, L.; Zhang, P.; El-Shall, H.; Moudgil, B.; Huang, X.; Zhang, L. Recovery of rare earth elements from phosphate rock by hydrometallurgical processes—A critical review. *Chem. Eng. J.* **2018**, *335*, 774–800. [CrossRef]
6. Zhang, B.; Liu, C.; Li, C.; Jiang, M. Separation and recovery of valuable metals from low-grade REE-Nb-Fe ore. *Int. J. Miner. Process.* **2016**, *150*, 16–23. [CrossRef]
7. Balaram, V. Rare earth elements: A review of applications, occurrence, exploration, analysis, recycling, and environmental impact. *Geosci. Front.* **2019**, *10*, 1285–1303. [CrossRef]
8. Sethurajan, M.; van Hullebusch, E.D.; Fontana, D.; Akcil, A.; Deveci, H.; Batinic, B.; Leal, J.P.; Gasche, T.A.; Kucuker, M.A.; Kuchta, K.; et al. Recent advances on hydrometallurgical recovery of critical and precious elements from end of life electronic wastes-a review. *Crit. Rev. Env. Sci. Technol.* **2019**, *49*, 212–275. [CrossRef]
9. Swain, N.; Mishra, S. A review on the recovery and separation of rare earths and transition metals from secondary resources. *J. Clean. Prod.* **2019**, *220*, 884–898. [CrossRef]
10. Spooren, J.; Atia, T.A. Combined microwave assisted roasting and leaching to recover platinum group metals from spent automotive catalysts. *Miner. Eng.* **2020**, *146*, 106153. [CrossRef]
11. Asadollahzadeh, M.; Torkaman, R.; Torab-Mostaedi, M.; Hemmati, A.; Ghaemi, A. Efficient recovery of neodymium and praseodymium from NdFeB magnet-leaching phase with and without ionic liquid as a carrier in the supported liquid membrane. *Chem. Pap.* **2020**, *74*, 4193–4201. [CrossRef]
12. Wu, S.; Zhao, L.; Wang, L.; Huang, X.; Zhang, Y.; Feng, Z.; Cui, D. Simultaneous recovery of rare earth elements and phosphorus from phosphate rock by phosphoric acid leaching and selective precipitation: Towards green process. *J. Rare Earths* **2019**, *37*, 652–658. [CrossRef]
13. Virolainen, S.; Repo, E.; Sainio, T. Recovering rare earth elements from phosphogypsum using a resin-in-leach process: Selection of resin, leaching agent, and eluent. *Hydrometallurgy* **2019**, *189*, 105125. [CrossRef]
14. Pavon, S.; Fortuny, A.; Call, M.T.; Sastre, A.M. Improved rare earth elements recovery from fluorescent lamp wastes applying supported liquid membranes to the leaching solutions. *Sep. Purif. Technol.* **2019**, *224*, 332–339. [CrossRef]
15. He, C.; Salih, K.A.; Wei, Y.; Mira, H.; Abdel-Rahman, A.A.-H.; Elwakeel, K.Z.; Hamza, M.F.; Guibal, E. Efficient recovery of rare earth elements (Pr (III) and Tm (III)) from mining residues using a new phosphorylated hydrogel (Algal Biomass/PEI). *Metals* **2021**, *11*, 294. [CrossRef]
16. Hamza, M.F.; Sallam, O.R.; Khalafalla, M.S.; Abbas, A.E.A.; Wei, Y. Geological and radioactivity studies accompanied by uranium recovery: Um Bogma Formation, southwestern Sinai, Egypt. *J. Radioanal. Nucl. Chem.* **2020**, *324*, 1039–1051. [CrossRef]
17. Khalafalla, M.S. Biotechnological recovery of uranium (VI) from Abu Zeneima spent ore residue using green lixiviant. *J. Radioanal. Nucl. Chem.* **2022**, *331*, 2503–2513. [CrossRef]
18. Abu Khoziem, H.; Khalafalla, M.; Abdellah, W. Green recovery of uranium from Abu Zeneima mineralised carbonaceous shale, West Central Sinai, Egypt. *Int. J. Environ. Anal. Chem.* **2021**, 1–12. [CrossRef]
19. Ni'am, A.C.; Wang, Y.-F.; Chen, S.-W.; Chang, G.-M.; You, S.-J. Simultaneous recovery of rare earth elements from waste permanent magnets (WPMs) leach liquor by solvent extraction and hollow fiber supported liquid membrane. *Chem. Eng. Process. Process Intensif.* **2020**, *148*, 107831. [CrossRef]
20. Pavon, S.; Fortuny, A.; Coll, M.T.; Sastre, A.M. Solvent extraction modeling of Ce/Eu/Y from chloride media using D2EHPA. *AIChE J.* **2019**, *65*, 16627. [CrossRef]
21. Pavon, S.; Fortuny, A.; Coll, M.T.; Sastre, A.M. Neodymium recovery from NdFeB magnet wastes using Primene 81R. Cyanex 572 IL by solvent extraction. *J. Environ. Manag.* **2018**, *222*, 359–367. [CrossRef]

22. Xia, Y.; Xiao, L.; Tian, J.; Li, Z.; Zeng, L. Recovery of rare earths from acid leach solutions of spent nickel-metal hydride batteries using solvent extraction. *J. Rare Earths* **2015**, *33*, 1348–1354. [CrossRef]
23. Hamza, M.F. Grafting of quaternary ammonium groups for uranium (VI) recovery: Application on natural acidic leaching liquor. *J. Radioanal. Nucl. Chem.* **2019**, *322*, 519–532. [CrossRef]
24. Hamza, M.F.; El-Aassy, I.E.; Guibal, E. Integrated treatment of tailing material for the selective recovery of uranium, rare earth elements and heavy metals. *Miner. Eng.* **2019**, *133*, 138–148. [CrossRef]
25. Khalafalla, M.S.; Abdellah, W.; Khoziem, H.; El-Hamid, A.; Abd Allh, M. Ecological treatment of El Kriymat boiler ash for recovering vanadium, nickel and zinc from sulfate leach liquor. *J. Mater. Cycles Waste Manag.* **2022**, *25*, 441–455. [CrossRef]
26. Hou, H.; Xu, J.; Wang, Y.; Chen, J. Solvent extraction of lanthanum and cerium ions from hydrochloric acidic aqueous solutions using partly saponified 2-ethylhexyl phosphonic acid mono-2-ethylhexyl ester. *Chin. J. Chem. Eng.* **2016**, *24*, 79–85. [CrossRef]
27. Huang, X.; Dong, J.; Wang, L.; Feng, Z.; Xue, Q.; Meng, X. Selective recovery of rare earth elements from ion-adsorption rare earth element ores by stepwise extraction with HEH(EHP) and HDEHP. *Green Chem.* **2017**, *19*, 1345–1352. [CrossRef]
28. Singh, D.K.; Anitha, M.; Kain, V. Development of solvent extraction process for erbium purification. *Sep. Sci. Technol.* **2017**, *52*, 2284–2290. [CrossRef]
29. Jorjani, E.; Shahbazi, M. The production of rare earth elements group via tributyl phosphate extraction and precipitation stripping using oxalic acid. *Arab. J. Chem.* **2016**, *9*, S1532–S1539. [CrossRef]
30. Abisheva, Z.S.; Karshigina, Z.B.; Bochevskaya, Y.G.; Akcil, A.; Sargelova, E.A.; Kvyatkovskaya, M.N.; Silachyov, I.Y. Recovery of rare earth metals as critical raw materials from phosphorus slag of long-term storage. *Hydrometallurgy* **2017**, *173*, 271–282. [CrossRef]
31. Hidayah, N.N.; Abidin, S.Z. The evolution of mineral processing in extraction of rare earth elements using liquid-liquid extraction: A review. *Miner. Eng.* **2018**, *121*, 146–157. [CrossRef]
32. Wu, S.; Wang, L.; Zhang, P.; El-Shall, H.; Moudgil, B.; Huang, X.; Zhao, L.; Zhang, L.; Feng, Z. Simultaneous recovery of rare earths and uranium from wet process phosphoric acid using solvent extraction with D2EHPA. *Hydrometallurgy* **2018**, *175*, 109–116. [CrossRef]
33. Reddy, B.R.; Kumar, J.R. Rare earths extraction, separation, and recovery from phosphoric acid media. *Solvent Extr. Ion Exch.* **2016**, *34*, 226–240. [CrossRef]
34. Agarwal, V.; Safarzadeh, M.S. Solvent extraction and separation of cerium(III) and samarium(III) from mixed rare earth solutions using PC88A. *Miner. Metall. Process.* **2017**, *34*, 125–131. [CrossRef]
35. Sharaf, M.; Yoshida, W.; Kubota, F.; Goto, M. Selective extraction of scandium by a long alkyl chain carboxylic acid/organophosphonic ester binary extractant. *Solvent Extr. Ion Exch.* **2018**, *36*, 647–657. [CrossRef]
36. Gomes, R.D.; Seruff, L.A.; Waineraich Scal, M.L.; Vera, Y.M. The Influence of lactic acid concentration on the separation of light rare earth elements by continuous liquid-liquid extraction with 2-ethylhexyl phosphonic acid mono-2-ethylhexyl ester. *Metall. Mater. Trans. B* **2018**, *49*, 460–465. [CrossRef]
37. Pavon, S.; Fortuny, A.; Coll, M.T.; Sastre, A.M. Rare earths separation from fluorescent lamp wastes using ionic liquids as extractant agents. *Waste Manag.* **2018**, *82*, 241–248. [CrossRef]
38. Erust, C.; Akcil, A.; Tuncuk, A.; Deveci, H.; Yazici, E.Y. A multi-stage process for recovery of neodymium (Nd) and dysprosium (Dy) from spent hard disc drives (HDDs). *Miner. Process. Extr. Metall. Rev.* **2019**, *42*, 90–101. [CrossRef]
39. Tunsu, C.; Petranikova, M.; Ekberg, C.; Retegan, T. A hydrometallurgical process for the recovery of rare earth elements from fluorescent lamp waste fractions. *Sep. Purif. Technol.* **2016**, *161*, 172–186. [CrossRef]
40. Rho, B.-J.; Sun, P.-P.; Cho, S.-Y. Recovery of neodymium and praseodymium from nitrate-based leachate of permanent magnet by solvent extraction with trioctylphosphine oxide. *Sep. Purif. Technol.* **2020**, *238*, 116429. [CrossRef]
41. Ang, K.L.; Li, D.; Nikoloski, A.N. The effectiveness of ion exchange resins in separating uranium and thorium from rare earth elements in acidic aqueous sulfate media. Part 2. Chelating resins. *Miner. Eng.* **2018**, *123*, 8–15. [CrossRef]
42. Kim, J.-G. Separation of heavy rare earth elements with extraction chromatography. *Curr. Nanosci.* **2014**, *10*, 11–15. [CrossRef]
43. Matsunaga, H.; Ismail, A.A.; Wakui, Y.; Yokoyama, T. Extraction of rare earth elements with 2-ethylhexyl hydrogen 2-ethylhexyl phosphonate impregnated resins having different morphology and reagent content. *React. Funct. Polym.* **2001**, *49*, 189–195. [CrossRef]
44. Mondal, S.; Ghar, A.; Satpati, A.K.; Sinharoy, P.; Singh, D.K.; Sharma, J.N.; Sreenivas, T.; Kain, V. Recovery of rare earth elements from coal fly ash using TEHDGA impregnated resin. *Hydrometallurgy* **2019**, *185*, 93–101. [CrossRef]
45. Kegl, T.; Kosak, A.; Lobnik, A.; Novak, Z.; Kralj, A.K.; Ban, I. Adsorption of rare earth metals from wastewater by nanomaterials: A review. *J. Hazard. Mater.* **2020**, *386*, 121632. [CrossRef]
46. Galhoum, A.A.; Mahfouz, M.G.; Abdel-Rehem, S.T.; Gomaa, N.A.; Atia, A.A.; Vincent, T.; Guibal, E. Diethylenetriamine-functionalized chitosan magnetic nano-based particles for the sorption of rare earth metal ions Nd(III), Dy(III) and Yb(III). *Cellulose* **2015**, *22*, 2589–2605. [CrossRef]
47. Galhoum, A.A.; Mafhouz, M.G.; Abdel-Rehem, S.T.; Gomaa, N.A.; Atia, A.A.; Vincent, T.; Guibal, E. Cysteine-functionalized chitosan magnetic nano-based particles for the recovery of light and heavy rare earth metals: Uptake kinetics and sorption isotherms. *Nanomaterials* **2015**, *5*, 154–179. [CrossRef]
48. Hamza, M.F.; Abdel-Rahman, A.A.H.; Guibal, E. Magnetic glutamine-grafted polymer for the sorption of U(VI), Nd(III) and Dy(III). *J. Chem. Technol. Biotechnol.* **2018**, *93*, 1790–1806. [CrossRef]

49. Callura, J.C.; Perkins, K.M.; Baltrus, J.P.; Washburn, N.R.; Dzombak, D.A.; Karamalidis, A.K. Adsorption kinetics, thermodynamics, and isotherm studies for functionalized lanthanide-chelating resins. *J. Colloid Interface Sci.* **2019**, *557*, 465–477. [CrossRef]
50. Page, M.J.; Soldenhoff, K.; Ogden, M.D. Comparative study of the application of chelating resins for rare earth recovery. *Hydrometallurgy* **2017**, *169*, 275–281. [CrossRef]
51. Hamza, M.F.; El Aassy, I.E.; Ahmed, F.Y.; Abdel-Rahman, A.A.H.; Atta, A.M. Separation of uranium and rare earth elements with high purity from low-grade gibbsite-bearing shale ore by different chelating resins. *J. Dispers. Sci. Technol.* **2012**, *33*, 482–489. [CrossRef]
52. Page, M.J.; Quinn, J.E.; Soldenhoff, K.H. The impact of sulfate ions on the ion exchange of rare earth elements. *Hydrometallurgy* **2019**, *186*, 12–20. [CrossRef]
53. Miller, D.D.; Siriwardane, R.; McIntyre, D. Anion structural effects on interaction of rare earth element ions with Dowex 50W X8 cation exchange resin. *J. Rare Earths* **2018**, *36*, 879–890. [CrossRef]
54. Heres, X.; Blet, V.; Di Natale, P.; Ouaattou, A.; Mazouz, H.; Dhiba, D.; Cuer, F. Selective extraction of rare earth elements from phosphoric acid by ion exchange resins. *Metals* **2018**, *8*, 682. [CrossRef]
55. Ang, K.L.; Li, D.; Nikoloski, A.N. The effectiveness of ion exchange resins in separating uranium and thorium from rare earth elements in acidic aqueous sulfate media. Part 1. Anionic and cationic resins. *Hydrometallurgy* **2017**, *174*, 147–155. [CrossRef]
56. Rychkov, V.N.; Kirillov, E.V.; Kirillov, S.V.; Bunkov, G.M.; Mashkovtsev, M.A.; Botalov, M.S.; Semenishchev, V.S.; Volkovich, V.A. Selective ion exchange recovery of rare earth elements from uranium mining solutions. In *Physics, Technologies and Innovation*; Rempel, A.A., Volkovich, V.A., Eds.; AIP Publishing LLC: Melville, NY, USA, 2016; Volume 1767.
57. Fila, D.; Hubicki, Z.; Kolodynska, D. Recovery of metals from waste nickel-metal hydride batteries using multifunctional Diphonix resin. *Adsorpt. J. Int. Ads. Soc.* **2019**, *25*, 367–382. [CrossRef]
58. Kumar, B.N.; Radhika, S.; Kantam, M.L.; Reddy, B.R. Solid-liquid extraction of terbium from phosphoric acid solutions using solvent-impregnated resin containing TOPS 99. *J. Chem. Technol. Biotechnol.* **2011**, *86*, 562–569. [CrossRef]
59. Kumar, B.N.; Radhika, S.; Reddy, B.R. Solid-liquid extraction of heavy rare-earths from phosphoric acid solutions using Tulsion CH-96 and T-PAR resins. *Chem. Eng. J.* **2010**, *160*, 138–144. [CrossRef]
60. Araucz, K.; Aurich, A.; Kolodynska, D. Novel multifunctional ion exchangers for metal ions removal in the presence of citric acid. *Chemosphere* **2020**, *251*, 12633. [CrossRef]
61. Roberts, G.A.F. *Chitin Chemistry*; Macmillan Publishers, Ltd.: London, UK, 1992; p. 350.
62. Guibal, E. Interactions of metal ions with chitosan-based sorbents: A review. *Sep. Purif. Technol.* **2004**, *38*, 43–74. [CrossRef]
63. Zhang, L.; Sellaoui, L.; Franco, D.; Dotto, G.L.; Bajahzar, A.; Belmabrouk, H.; Bonilla-Petriciolet, A.; Oliveira, M.L.S.; Li, Z. Adsorption of dyes brilliant blue, sunset yellow and tartrazine from aqueous solution on chitosan: Analytical interpretation via multilayer statistical physics model. *Chem. Eng. J.* **2020**, *382*, 122952. [CrossRef]
64. Hamza, M.F.; Alotaibi, S.H.; Wei, Y.; Mashaal, N.M. High-Performance Hydrogel Based on Modified Chitosan for Removal of Heavy Metal Ions in Borehole: A Case Study from the Bahariya Oasis, Egypt. *Catalysts* **2022**, *12*, 721. [CrossRef]
65. Hamza, M.F.; Wei, Y.; Althumayri, K.; Fouda, A.; Hamad, N.A. Synthesis and Characterization of Functionalized Chitosan Nanoparticles with Pyrimidine Derivative for Enhancing Ion Sorption and Application for Removal of Contaminants. *Materials* **2022**, *15*, 4676. [CrossRef] [PubMed]
66. Hamza, M.F.; Hamad, N.A.; Hamad, D.M.; Khalafalla, M.S.; Abdel-Rahman, A.A.-H.; Zeid, I.F.; Wei, Y.; Hessien, M.M.; Fouda, A.; Salem, W.M. Synthesis of eco-friendly biopolymer, alginate-chitosan composite to adsorb the heavy metals, Cd (II) and Pb (II) from contaminated effluents. *Materials* **2021**, *14*, 2189. [CrossRef] [PubMed]
67. Gandhi, M.R.; Meenakshi, S. Preparation and characterization of La(III) encapsulated silica gel/chitosan composite and its metal uptake studies. *J. Hazard. Mater.* **2012**, *203*, 29–37. [CrossRef]
68. Mahmoud, M.E.; Ibrahim, G.A.; Abdelwahab, M.S. Manganese dioxide nanoparticles decorated with chitosan for effective removal of lead and lanthanum ions from water by microwave sorption technique. *Mater. Sci. Eng. B* **2021**, *267*, 115091. [CrossRef]
69. Ali, I.; Zakaria, E.; Khalil, M.; El-Tantawy, A.; El-Saied, F. Synthesis of ion-imprinted polymers based on chitosan for high selectivity of La(III), Ce (III) and Sm (III) via solid phase extraction. *J. Mol. Liq.* **2022**, *356*, 119058. [CrossRef]
70. Lopez-Ramon, M.V.; Stoeckli, F.; Moreno-Castilla, C.; Carrasco-Marin, F. On the characterization of acidic and basic surface sites on carbons by various techniques. *Carbon* **1999**, *37*, 1215–1221. [CrossRef]
71. Nayak, A.K.; Pal, A. Development and validation of an adsorption kinetic model at solid-liquid interface using normalized Gudermannian function. *J. Mol. Liq.* **2019**, *276*, 67–77. [CrossRef]
72. Hamza, M.F.; Guibal, E.; Wei, Y.; Fouda, A. Magnetic amino-sulfonic dual sorbent for uranyl sorption from aqueous solutions–Influence of light irradiation on sorption properties. *Chem. Eng. J.* **2022**, *456*, 141099. [CrossRef]
73. Ali, I.; Nassar, M.Y.; Kotp, Y.H.; Khalil, M. Cylindrical-design, dehydration, and sorption properties of easily synthesized magnesium phosphosilicate nanopowder. *Part. Sci. Technol.* **2019**, *37*, 207–219. [CrossRef]
74. Zhan, W.; Xu, C.H.; Qian, G.F.; Huang, G.H.; Tang, X.Z.; Lin, B.F. Adsorption of Cu(II), Zn(II), and Pb(II) from aqueous single and binary metal solutions by regenerated cellulose and sodium alginate chemically modified with polyethyleneimine. *RSC Adv.* **2018**, *8*, 18723–18733. [CrossRef] [PubMed]
75. Hamza, M.F.; Abdel-Rahman, A.A.H. Extraction studies of some hazardous metal ions using magnetic peptide resins. *J. Dispers. Sci. Technol.* **2015**, *36*, 411–422. [CrossRef]

76. Hamza, M.F.; Aly, M.M.; Abdel-Rahman, A.A.H.; Ramadan, S.; Raslan, H.; Wang, S.; Vincent, T.; Guibal, E. Functionalization of magnetic chitosan particles for the sorption of U(VI), Cu(II) and Zn(II)—Hydrazide derivative of glycine-grafted chitosan. *Materials* **2017**, *10*, 539. [CrossRef] [PubMed]
77. Coates, J. Interpretation of Infrared Spectra, A Practical Approach. In *Encyclopedia of Analytical Chemistry*; Meyers, R.A., Ed.; John Wiley & Sons Ltd.: Chichester, UK, 2000; pp. 10815–10837.
78. Colthup, N.B.; Daly, L.H.; Wiberley, S.E. *Introduction to Infrared and Raman Spectroscopy*, 3rd ed.; Academic Press, Inc.: San Diego, CA, USA, 1990; p. 560.
79. Hu, X.J.; Wang, J.S.; Liu, Y.G.; Li, X.; Zeng, G.M.; Bao, Z.L.; Zeng, X.X.; Chen, A.W.; Long, F. Adsorption of chromium (VI) by ethylenediamine-modified cross-linked magnetic chitosan resin: Isotherms, kinetics and thermodynamics. *J. Hazard. Mater.* **2011**, *185*, 306–314. [CrossRef]
80. Chen, Y.; Geng, J.; Zhuang, Y.; Zhao, J.; Chu, L.; Luo, X.; Zhao, Y.; Guo, Y. Preparation of the chitosan grafted poly (quaternary ammonium)/Fe_3O_4 nanoparticles and its adsorption performance for food yellow 3. *Carbohydr. Polym.* **2016**, *152*, 327–336. [CrossRef]
81. Lin-Vien, D.; Colthup, N.B.; Fateley, W.G.; Grasselli, J.G. CHAPTER 16—Organophosphorus Compounds. In *The Handbook of Infrared and Raman Characteristic Frequencies of Organic Molecules*; Lin-Vien, D., Colthup, N.B., Fateley, W.G., Grasselli, J.G., Eds.; Academic Press: San Diego, CA, USA, 1991; pp. 263–276.
82. Coates, J. Interpretation of Infrared Spectra, A Practical Approach. In *Encyclopedia of Analytical Chemistry*; John Wiley & Sons, Ltd.: Hoboken, NJ, USA, 2006; pp. 1–23.
83. Hagab, R.H.; Kotp, Y.H.; Eissa, D. Using nanotechnology for enhancing phosphorus fertilizer use efficiency of peanut bean grown in sandy soils. *J. Adv. Pharm. Educ. Res.* **2018**, *8*, 59–67.
84. Hamza, M.F.; Guibal, E.; Abdel-Rahman, A.A.-H.; Salem, M.; Khalafalla, M.S.; Wei, Y.; Yin, X. Enhancement of Cerium Sorption onto Urea-Functionalized Magnetite Chitosan Microparticles by Sorbent Sulfonation—Application to Ore Leachate. *Molecules* **2022**, *27*, 7562. [CrossRef]
85. Hamza, M.F.; Fouda, A.; Wei, Y.; El Aassy, I.E.; Alotaibi, S.H.; Guibal, E.; Mashaal, N.M. Functionalized biobased composite for metal decontamination–Insight on uranium and application to water samples collected from wells in mining areas (Sinai, Egypt). *Chem. Eng. J.* **2022**, *431*, 133967. [CrossRef]
86. Hamza, M.F.; Abdel-Rahman, A.A.-H.; Negm, A.S.; Hamad, D.M.; Khalafalla, M.S.; Fouda, A.; Wei, Y.; Amer, H.H.; Alotaibi, S.H.; Goda, A.E.-S. Grafting of Thiazole Derivative on Chitosan Magnetite Nanoparticles for Cadmium Removal—Application for Groundwater Treatment. *Polymers* **2022**, *14*, 1240. [CrossRef]
87. Hamza, M.F.; Guibal, E.; Althumayri, K.; Wei, Y.; Eid, A.M.; Fouda, A. Poly-condensation of N-(2-acetamido)-2-aminoethanesulfonic acid with formaldehyde for the synthesis of a highly efficient sorbent for Cs (I). *Chem. Eng. J.* **2022**, *454*, 140155. [CrossRef]
88. Hamza, M.F.; Mahfouz, M.G.; Abdel-Rahman, A.A.-H. Adsorption of uranium (VI) ions on hydrazinyl amine and 1, 3, 4-thiadiazol-2 (3 H)-thion chelating resins. *J. Dispers. Sci. Technol.* **2012**, *33*, 1544–1551. [CrossRef]
89. Hamza, M.F.; Abu Khoziem, H.A.; Khalafalla, M.S.; Abdellah, W.M.; Zaki, D.I.; Althumayri, K.; Wei, Y. Ecofriendly Composite as a Promising Material for Highly-Performance Uranium Recovery from Different Solutions. *Toxics* **2022**, *10*, 490. [CrossRef] [PubMed]
90. Zhang, S.; Huang, Q.; Chen, L.; Zhang, W.; Yin, X.; Hamza, M.; Wei, Y.; Ning, S. Efficient Separation of Strontium in Different Environments with Novel Acid-Resistant Silica-Based Ion Exchange Resin. Available online: https://papers.ssrn.com/sol3/papers.cfm?abstract_id=4335796 (accessed on 3 January 2023). [CrossRef]
91. Kolodynska, D.; Fila, D.; Hubicki, Z. Static and dynamic studies of lanthanum(III) ion adsorption/desorption from acidic solutions using chelating ion exchangers with different functionalities. *Environ. Res.* **2020**, *191*, 110171. [CrossRef]
92. Wei, Y.; Salih, K.A.; Hamza, M.F.; Fujita, T.; Rodríguez-Castellón, E.; Guibal, E. Synthesis of a new phosphonate-based sorbent and characterization of its interactions with lanthanum (Iii) and terbium (iii). *Polymers* **2021**, *13*, 1513. [CrossRef] [PubMed]
93. Pearson, R.G. Acids and bases. *Science* **1966**, *151*, 172–177. [CrossRef]
94. Rafik, B.; Noureddine, O.; Abderabbou, A.; Habib, L. Self-diffusion coefficients of the trivalent f-element ion series in dilute and moderately dilute aqueous solutions: A comparative study between europium, gadolinium, terbium and berkelium. In *Actinides 2009*; Rao, L., Tobin, J.G., Shuh, D.K., Eds.; IOP Conference Series-Materials Science and Engineering: Bristol, UK, 2010; Volume 9.
95. Yang, Y.J.; Alexandratos, S.D. Affinity of polymer-supported reagents for lanthanides as a function of donor atom polarizability. *Ind. Eng. Chem. Res.* **2009**, *48*, 6173–6187. [CrossRef]
96. Alexandratos, S.D.; Zhu, X. The effect of hydrogen bonding in enhancing the ionic affinities of immobilized monoprotic phosphate ligands. *Materials* **2017**, *10*, 968. [CrossRef]
97. Khalil, M.M.H.; Atrees, M.S.; Abd El Fatah, A.I.L.; Salem, H.; Roshdi, R. Synthesis and application studies of chitosan acryloylthiourea derivative for the separation of rare earth elements. *J. Dispers. Sci. Technol.* **2018**, *39*, 605–613. [CrossRef]
98. Elwakeel, K.Z.; Daher, A.M.; Abd El-Fatah, A.I.L.; Abd El Monem, H.; Khalil, M.M.H. Biosorption of lanthanum from aqueous solutions using magnetic alginate beads. *J. Dispers. Sci. Technol.* **2017**, *38*, 145–151. [CrossRef]
99. Mahmoud, M.E.; Mohamed, A.K.; Amira, M.F.; Seleim, S.M. Water-stable metal-organic framework/amine-modified silica/poly (piperazine-cresol) hybrids for efficient uptake of La(III) ions. *Mater. Chem. Phys.* **2020**, *251*, 123107. [CrossRef]
100. Wei, Y.; Salih, K.A.; Hamza, M.F.; Castellón, E.R.; Guibal, E. Novel phosphonate-functionalized composite sorbent for the recovery of lanthanum (III) and terbium (III) from synthetic solutions and ore leachate. *Chem. Eng. J.* **2021**, *424*, 130500. [CrossRef]

101. Texier, A.C.; Andrès, Y.; Le Cloirec, P. Selective biosorption of lanthanide (La, Eu) ions by Mycobacterium smegmatis. *Environ. Technol.* **1997**, *18*, 835–841. [CrossRef]
102. Torab-Mostaedi, M. Biosorption of lanthanum and cerium from aqueous solutions using tangerine (Citrus reticulate) peel: Equilibrium, kinetic and thermodynamic studies. *Chem. Ind. Chem. Eng. Q.* **2013**, *19*, 79–88. [CrossRef]
103. Esma, B.; Omar, A.; Amine, D.M. Comparative study on lanthanum(III) sorption onto Lewatit TP 207 and Lewatit TP 260. *J. Radioanal. Nucl. Chem.* **2014**, *299*, 439–446. [CrossRef]
104. Hong, G.; Wang, M.; Li, X.; Shen, L.; Wang, X.; Zhu, M.; Hsiao, B.S. Micro-nano structure nanofibrous p-sulfonatocalix 8 arene complex membranes for highly efficient and selective adsorption of lanthanum(III) ions in aqueous solution. *RSC Adv.* **2015**, *5*, 21178–21188. [CrossRef]
105. Abu Elgoud, E.M.; Ismail, Z.H.; Ahmad, M.I.; El-Nadi, Y.A.; Abdelwahab, S.M.; Aly, H.F. Sorption of lanthanum(III) and neodymium(III) from concentrated phosphoric acid by strongly acidic cation exchange resin (SQS-6). *Russ. J. Appl. Chem.* **2019**, *92*, 1581–1592. [CrossRef]
106. Wu, D.; Zhao, J.; Zhang, L.; Wu, Q.; Yang, Y. Lanthanum adsorption using iron oxide loaded calcium alginate beads. *Hydrometallurgy* **2010**, *101*, 76–83. [CrossRef]
107. Vijayaraghavan, K.; Sathishkumar, M.; Balasubramanian, R. Biosorption of lanthanum, cerium, europium, and ytterbium by a brown marine alga, *Turbinaria conoides* . *Ind. Eng. Chem. Res.* **2010**, *49*, 4405–4411. [CrossRef]
108. Diniz, V.; Volesky, B. Effect of counterions on lanthanum biosorption by *Sargassum polycystum* . *Water Res.* **2005**, *39*, 2229–2236. [CrossRef]
109. Torab-Mostaedi, M.; Asadollahzadeh, M.; Hemmati, A.; Khosravi, A. Biosorption of lanthanum and cerium from aqueous solutions by grapefruit peel: Equilibrium, kinetic and thermodynamic studies. *Res. Chem. Intermed.* **2013**, *41*, 559–573. [CrossRef]
110. Sert, Ş.; Kütahyali, C.; İnan, S.; Talip, Z.; Çetinkaya, B.; Eral, M. Biosorption of lanthanum and cerium from aqueous solutions by *Platanus orientalis* leaf powder. *Hydrometallurgy* **2008**, *90*, 13–18. [CrossRef]
111. Rahman, M.M.; Khan, S.B.; Marwani, H.M.; Asiri, A.M. SnO_2-TiO_2 nanocomposites as new adsorbent for efficient removal of La(III) ions from aqueous solutions. *J. Taiwan Inst. Chem. Eng.* **2014**, *45*, 1964–1974. [CrossRef]
112. Oliveira, R.C.; Garcia, O., Jr. Study of biosorption of rare earth metals (La, Nd, Eu, Gd) by *Sargassum* sp biomass in batch systems: Physicochemical evaluation of kinetics and adsorption models. In *Biohydrometallurgy: A Meeting Point between Microbial Ecology, Metal Recovery Processes and Environmental Remediation*; Donati, E.R., Viera, M.R., Tavani, E.L., Giaveno, M.A., Lavalle, T.L., Chiacchiarini, P.A., Eds.; Advanced Materials Research; Trans Tech Publications: Wollerau, Switzerland, 2009; Volume 71–73, pp. 605–608.
113. Chen, Q. Study on the adsorption of lanthanum(III) from aqueous solution by bamboo charcoal. *J. Rare Earths* **2010**, *28*, 125–131. [CrossRef]
114. Oyewo, O.A.; Onyango, M.S.; Wolkersdorfer, C. Lanthanides removal from mine water using banana peels nanosorbent. *Int. J. Environ. Sci. Technol.* **2018**, *15*, 1265–1274. [CrossRef]
115. Oral, A.E.; Aytas, S.; Yusan, S.; Sert, S.; Gok, C.; Elmastas Gultekin, O. Preparation and characterization of a graphene-based magnetic nanocomposite for the adsorption of lanthanum ions from aqueous solution. *Anal. Lett.* **2020**, *53*, 1812–1833. [CrossRef]
116. Philip, L.; Iyengar, L.; Venkobachar, C. Biosorption of U, La, Pr, Nd, Eu and Dy by *Pseudomonas aeruginosa* . *J. Ind. Microbiol. Biotechnol.* **2000**, *25*, 1–7. [CrossRef]
117. Tien, C. *Adsorption Calculations and Modeling*; Butterworth-Heinemann: Newton, MA, USA, 1994; p. 243. [CrossRef]
118. Lima, É.C.; Dehghani, M.H.; Guleria, A.; Sher, F.; Karri, R.R.; Dotto, G.L.; Tran, H.N. CHAPTER 3 - Adsorption: Fundamental aspects and applications of adsorption for effluent treatment. In *Green Technologies for the Defluoridation of Water*; Elsevier: Amsterdam, The Netherlands, 2021; pp. 41–88. [CrossRef]
119. Buema, G.; Lupu, N.; Chiriac, H.; Ciobanu, G.; Bucur, R.D.; Bucur, D.; Favier, L.; Harja, M. Performance assessment of five adsorbents based on fly ash for removal of cadmium ions. *J. Mol. Liq.* **2021**, *333*, 115932. [CrossRef]
120. Crank, J. *The Mathematics of Diffusion, 2nd. ed.*; Oxford University Press: Oxford, UK, 1975; p. 414.
121. Ho, Y.S.; McKay, G. Pseudo-second order model for sorption processes. *Process Biochem.* **1999**, *34*, 451–465. [CrossRef]
122. Hamza, M.F.; Guibal, E.; Althumayri, K.; Vincent, T.; Yin, X.; Wei, Y.; Li, W. New Process for the Sulfonation of Algal/PEI Biosorbent for Enhancing Sr (II) Removal from Aqueous Solutions—Application to Seawater. *Molecules* **2022**, *27*, 7128. [CrossRef]
123. Fouda, A.; Hassan, S.E.-D.; Eid, A.M.; Awad, M.A.; Althumayri, K.; Badr, N.F.; Hamza, M.F. Endophytic bacterial strain, Brevibacillus brevis-mediated green synthesis of copper oxide nanoparticles, characterization, antifungal, in vitro cytotoxicity, and larvicidal activity. *Green Process. Synth.* **2022**, *11*, 931–950. [CrossRef]
124. Fouda, A.; Hamza, M.F.; Shaheen, T.I.; Wei, Y. Nanotechnology and smart textiles: Sustainable developments of applications. *Front. Bioeng. Biotechnol.* **2022**, *10*. [CrossRef]
125. Amin, M.A.; Ismail, M.A.; Badawy, A.A.; Awad, M.A.; Hamza, M.F.; Awad, M.F.; Fouda, A. The Potency of fungal-fabricated selenium nanoparticles to improve the growth performance of Helianthus annuus L. and control of cutworm Agrotis ipsilon. *Catalysts* **2021**, *11*, 1551. [CrossRef]
126. Hassan, S.E.-D.; Fouda, A.; Saied, E.; Farag, M.M.; Eid, A.M.; Barghoth, M.G.; Awad, M.A.; Hamza, M.F.; Awad, M.F. Rhizopus Oryzae-mediated green synthesis of magnesium oxide nanoparticles (MgO-NPs): A promising tool for antimicrobial, mosquitocidal action, and tanning effluent treatment. *J. Fungi* **2021**, *7*, 372. [CrossRef]
127. Fouda, A.; Eid, A.M.; Guibal, E.; Hamza, M.F.; Hassan, S.E.-D.; Alkhalifah, D.H.M.; El-Hossary, D. Green Synthesis of Gold Nanoparticles by Aqueous Extract of Zingiber officinale: Characterization and Insight into Antimicrobial, Antioxidant, and In Vitro Cytotoxic Activities. *Appl. Sci.* **2022**, *12*, 12879. [CrossRef]

128. Fouda, A.; Hassan, S.E.-D.; Saied, E.; Hamza, M.F. Photocatalytic degradation of real textile and tannery effluent using biosynthesized magnesium oxide nanoparticles (MgO-NPs), heavy metal adsorption, phytotoxicity, and antimicrobial activity. *J. Environ. Chem. Eng.* **2021**, *9*, 105346. [CrossRef]
129. Fouda, A.; Hassan, S.E.-D.; Eid, A.M.; Abdel-Rahman, M.A.; Hamza, M.F. Light enhanced the antimicrobial, anticancer, and catalytic activities of selenium nanoparticles fabricated by endophytic fungal strain, Penicillium crustosum EP-1. *Sci. Rep.* **2022**, *12*, 1–16. [CrossRef]
130. Hamza, M.F.; Khalafalla, M.S.; Wei, Y.; Hamad, N.A. Effect of bi-functionalization silica micro beads on uranium adsorption from synthetic and washing pregnant uranyl solutions. *J. Radioanal. Nucl. Chem.* **2021**, *330*, 191–206. [CrossRef]
131. Hamza, M.F.; El Aassy, I.E. Solid phase extraction of uranium removal from underground water, Wadi Naseib, Southwestern Sinai, Egypt. *Desalination Water Treat.* **2014**, *52*, 331–338. [CrossRef]
132. Fouda, A.; Awad, M.A.; Eid, A.M.; Saied, E.; Barghoth, M.G.; Hamza, M.F.; Awad, M.F.; Abdelbary, S.; Hassan, S.E.-D. An eco-friendly approach to the control of pathogenic microbes and Anopheles stephensi malarial vector using magnesium oxide nanoparticles (Mg-nps) fabricated by Penicillium chrysogenum. *Int. J. Mol. Sci.* **2021**, *22*, 5096. [CrossRef]
133. Hamza, M.F. Removal of uranium (VI) from liquid waste of calcareous shale, Allouga, southwestern Sinai, Egypt. *Desalination Water Treat.* **2015**, *54*, 2530–2540. [CrossRef]
134. Mohammadi, N.; Ganesan, A.; Chantler, C.T.; Wang, F. Differentiation of ferrocene D5d and D5h conformers using IR spectroscopy. *J. Organomet. Chem.* **2012**, *713*, 51–59. [CrossRef]
135. Fouda, A.; Eid, A.M.; Abdel-Rahman, M.A.; El-Belely, E.F.; Awad, M.A.; Hassan, S.E.-D.; Al-Faifi, Z.E.; Hamza, M.F. Enhanced antimicrobial, cytotoxicity, larvicidal, and repellence activities of brown algae, cystoseira crinita-mediated green synthesis of magnesium oxide nanoparticles. *Front. Bioeng. Biotechnol.* **2022**, *10*. [CrossRef]
136. Hamza, M.F. Uranium recovery from concentrated chloride solution produced from direct acid leaching of calcareous shale, Allouga ore materials, southwestern Sinai, Egypt. *J. Radioanal. Nucl. Chem.* **2018**, *315*, 613–626. [CrossRef]
137. Lord, R.C. Introduction to Infrared and Raman Spectroscopy. *J. Am. Chem. Soc.* **1965**, *87*, 1155–1156. [CrossRef]
138. Hamza, M.F.; Wei, Y.; Khalafalla, M.S.; Abed, N.S.; Fouda, A.; Elwakeel, K.Z.; Guibal, E.; Hamad, N.A. U (VI) and Th (IV) recovery using silica beads functionalized with urea-or thiourea-based polymers–Application to ore leachate. *Sci. Total Environ.* **2022**, *821*, 153184. [CrossRef]
139. Dai, X.; Nhung, N.T.H.; Hamza, M.F.; Guo, Y.; Chen, L.; He, C.; Ning, S.; Wei, Y.; Dodbiba, G.; Fujita, T. Selective adsorption and recovery of scandium from red mud leachate by using phosphoric acid pre-treated pitaya peel biochar. *Sep. Purif. Technol.* **2022**, *292*, 121043. [CrossRef]
140. Fouda, A.; Salem, S.S.; Wassel, A.R.; Hamza, M.F.; Shaheen, T.I. Optimization of green biosynthesized visible light active CuO/ZnO nano-photocatalysts for the degradation of organic methylene blue dye. *Heliyon* **2020**, *6*, e04896. [CrossRef]
141. Zhao, Z.; Xie, X.; Wang, Z.; Tao, Y.; Niu, X.; Huang, X.; Liu, L.; Li, Z. Immobilization of Lactobacillus rhamnosus in mesoporous silica-based material: An efficiency continuous cell-recycle fermentation system for lactic acid production. *J. Biosci. Bioeng.* **2016**, *121*, 645–651. [CrossRef]
142. Hamza, M.F.; Adel, A.-H.; Hawata, M.A.; El Araby, R.; Guibal, E.; Fouda, A.; Wei, Y.; Hamad, N.A. Functionalization of magnetic chitosan microparticles–Comparison of trione and trithione grafting for enhanced silver sorption and application to metal recovery from waste X-ray photographic films. *J. Environ. Chem. Eng.* **2022**, 107939. [CrossRef]
143. Hamza, M.F.; Goda, A.E.-S.; Ning, S.; Mira, H.I.; Abdel-Rahman, A.A.-H.; Wei, Y.; Fujita, T.; Amer, H.H.; Alotaibi, S.H.; Fouda, A. Photocatalytic Efficacy of Heterocyclic Base Grafted Chitosan Magnetite Nanoparticles on Sorption of Pb (II); Application on Mining Effluent. *Catalysts* **2022**, *12*, 330. [CrossRef]
144. Hamza, M.F.; Mira, H.; Wei, Y.; Aboelenin, S.M.; Guibal, E.; Salem, W.M. Sulfonation of chitosan for enhanced sorption of Li (I) from acidic solutions–Application to metal recovery from waste Li-ion mobile battery. *Chem. Eng. J.* **2022**, *441*, 135941. [CrossRef]
145. Fouda, A.; Awad, M.A.; AL-Faifi, Z.E.; Gad, M.E.; Al-Khalaf, A.A.; Yahya, R.; Hamza, M.F. Aspergillus flavus-Mediated Green Synthesis of Silver Nanoparticles and Evaluation of Their Antibacterial, Anti-Candida, Acaricides, and Photocatalytic Activities. *Catalysts* **2022**, *12*, 462. [CrossRef]
146. Hamza, M.F.; Salih, K.A.; Zhou, K.; Wei, Y.; Khoziem, H.A.A.; Alotaibi, S.H.; Guibal, E. Effect of bi-functionalization of algal/polyethyleneimine composite beads on the enhancement of tungstate sorption: Application to metal recovery from ore leachate. *Sep. Purif. Technol.* **2022**, *290*, 120893. [CrossRef]
147. Zahra, M.H.; Hamza, M.F.; El-Habibi, G.; Abdel-Rahman, A.A.-H.; Mira, H.I.; Wei, Y.; Alotaibi, S.H.; Amer, H.H.; Goda, A.E.-S.; Hamad, N.A. Synthesis of a Novel Adsorbent Based on Chitosan Magnetite Nanoparticles for the High Sorption of Cr (VI) ions: A Study of Photocatalysis and Recovery on Tannery Effluents. *Catalysts* **2022**, *12*, 678. [CrossRef]
148. Hamza, M.F.; Hamad, D.M.; Hamad, N.A.; Adel, A.-H.; Fouda, A.; Wei, Y.; Guibal, E.; El-Etrawy, A.-A.S. Functionalization of magnetic chitosan microparticles for high-performance removal of chromate from aqueous solutions and tannery effluent. *Chem. Eng. J.* **2022**, *428*, 131775. [CrossRef]